PEM Fuel Cells and Platinum-Based Electrocatalysts

Junliang Zhang
Fuel Cell Business, General Motors Global Propulsion Systems, Pontiac, MI, USA

Article Outline

Glossary
Definition of the Subject
Introduction
Electrocatalysis of the ORR at Platinum Surfaces
Pt-Alloy Electrocatalysts
Pt Monolayer Electrocatalysts
Pt and Pt-Alloy Nanowire and Nanotube Electrocatalysts
Facet- and Shape-Controlled Pt-Alloy Nanocrystal Electrocatalysts
Future Directions
Bibliography

Glossary

Anode An electrode where the electrochemical oxidation reaction(s) occurs, generating free electrons that flow through a polarized electrical device and enter the cathode. In a fuel cell, the fuel oxidation reaction happens at the anode.

Cathode An electrode where the electrochemical reduction reaction(s) occurs, by consuming the electrons originated from the anode. In a fuel cell, the oxygen reduction reaction happens at the cathode.

Electrocatalyst A material that is applied on the surface of an electrode to catalyze half-cell reactions.

Normal hydrogen electrode (NHE) Also known as the standard hydrogen electrode (SHE), it is a redox reference electrode which forms the basis of the thermodynamic scale of oxidation-reduction potentials. The potential of the NHE is defined as zero and based on equilibrium of the following redox half-cell reaction, typically on a Pt surface: $2H^+(aq) + 2e^- \rightarrow H_2(g)$ The activities of both the reduced form and the oxidized form are maintained at unity. That implies that the pressure of hydrogen gas is 1 atms and the concentration of hydrogen ions in the solution is 1 M.

Oxygen reduction reaction (ORR) An electrode reaction, in which oxygen gas is reduced at the cathode of an electrochemical cell. The product of the reaction can be water molecules, hydroxyl ions (OH^-), or sometimes hydrogen peroxide molecules. It is a very important and much-studied electrochemical reaction because it occurs at the cathode of practically all fuel cells.

Proton-exchange membrane fuel cells (PEMFC) Also known as polymer electrolyte membrane fuel cells, these are a type of fuel cells that use proton-conducting-ionomer membrane as the electrolyte to separate anode and cathode. Their distinguishing features include low operating temperature (<80 °C), high power density, quick start-up, and quick match to shifting demands for power. They are being developed for transport applications as well as stationary and portable applications.

Pt mass activity The kinetic current of the oxygen reduction reaction normalized by the mass of Pt metal contained in the electrocatalyst.

Pt-specific activity The kinetic current of the oxygen reduction reaction normalized by the electrochemical surface area of the Pt metal contained in the electrocatalyst.

Reversible hydrogen electrode (RHE) This differs from the NHE by the fact that the hydrogen-ion concentration of RHE reaction is the same as that in the actual electrolyte solution used for the working electrode. The potential of RHE is therefore (−0.059* (pH of the electrolyte)) V.

T. E. Lipman, A. Z. Weber (eds.), *Fuel Cells and Hydrogen Production*,
https://doi.org/10.1007/978-1-4939-7789-5_147

Originally published in
R. A. Meyers (ed.), *Encyclopedia of Sustainability Science and Technology*, © Springer Science+Business Media LLC 2017
https://doi.org/10.1007/978-1-4939-2493-6_147-3

Definition of the Subject

H_2/air-powered PEM fuel cells are a future substitute for combustion engines as the green power source for transport application. In PEM fuel cells, because of their low operating temperature and low pH, both anode and cathode reactions are catalyzed by Pt or Pt-based electrocatalysts. Pt is a precious and expensive noble metal, and therefore its loading requirement plays a major role in determining the cost of fuel cells in mass production. The anode hydrogen oxidation reaction on Pt is intrinsically fast and requires very little Pt, while the cathode oxygen reduction reaction (ORR) is a very sluggish reaction that consumes about 90% of the total Pt content in PEM fuel cells. The current Pt loading in the most advanced fuel cell vehicles that use state-of-the-art Pt-based catalysts is about four- to eight-fold higher than the target established for mass-produced fuel cell vehicles. Therefore, lowering the Pt loading at the cathode is the most critical mission for the PEM fuel cell development. To do that, significant depth of knowledge in understanding the ORR on Pt and Pt-based electrocatalysts' surfaces is required; and the search for novel Pt-based electrocatalysts with enhanced ORR activity is seemingly the most productive pathway.

Introduction

Ever since 1839, when Sir William Robert Grove introduced the first concept of fuel cells [1, 2], researchers have been continuously trying to apply fuel cells for stationary and mobile power sources [3, 4], because of their high energy efficiency and low environmental footprint. Fuel cells can be customarily classified according to the electrolyte employed, with different electrolytes operating at different temperature ranges. The operating temperature then dictates the types of fuels and electrode materials that can be used in a fuel cell. For example, aqueous electrolytes are limited to operating temperatures of about 200 °C or lower because of their high water vapor pressure. At these temperatures the fuel is, in applications requiring high current density and low cost, restricted to hydrogen. To accommodate the slow kinetics of the electrochemical reactions at such low temperature in acid environments, platinum catalysts are required for both cathode and anode. In high temperature fuel cells, CO or even CH_4 can be used as the fuel, and the catalyst is not necessary to be noble metals, because of the inherently fast electrode reaction kinetics.

Among various types of fuel cells, proton exchange membrane fuel cells (PEMFCs) have attracted the most attention in recent years due to their low operating temperature (about 80 °C), high power density, quick start-up, and quick match to shifting demands for power [3]. Hydrogen/air-powered PEMFCs make them the primary candidate for the power source of light-duty vehicles and buildings. In a recent study by Thomas [5], the author compared fuel cell and battery as the power sources for all-electric vehicles, and found that for any vehicle range greater than 160 km (100 miles), fuel cells are superior than batteries in terms of mass, volume, cost, initial greenhouse gas reductions, refueling time, well-to-wheel energy efficiency (using natural gas and biomass as the source) and life cycle costs. PEMFCs also allow direct use of methanol without a processor, called DMFC. DMFCs are the primary candidates for portable electronic applications; low power densities and high Pt requirements have precluded their use in vehicles to date.

One difficult challenge to make PEMFC vehicles cost-competitive with traditional combustion engine cars is the high platinum catalyst loading and poor catalyst durability of the fuel cells [6, 7]. In the mid- to late-1980s and in the early 1990s, the fuel cell team at Los Alamos National Laboratory (LANL) succeeded in demonstrating high performance H_2/air fuel cells with a platinum loading less than 0.5 mg Pt/cm^2 per electrode, which was one magnitude lower than its previous level [8–11]. In that effort, Raistrick [8] was the first one to cast ionomer into the electrocatalyst layer by impregnating a Pt/C electrode into the ionomer solution before hot-pressing it onto the membrane, and thus greatly increased the electrocatalyst-electrolyte interfacial contact area. Wilson et al. [9–11] improved that process by mixing the Pt/C powder catalyst with ionomer solution before coating the electrode. Those

research achievements at LANL partly led to the renaissance in PEMFCs in the past 2 decades [4].

In a PEMFC, if pure hydrogen is used as fuel, the anode reaction is then the hydrogen oxidation reaction (HOR) at the surface of the anode platinum electrocatalyst. The hydrogen oxidation reaction (HOR) and hydrogen evolution reaction (HER) are by far the most thoroughly investigated electrochemical reaction system [12]. Due to the fast electrode kinetics of hydrogen oxidation at platinum surface [12–14], the anode platinum loading can be reduced down to 0.05 mg Pt/cm^2 without significant performance loss [15]. The cathode reaction in a PEM fuel cell is the oxygen reduction reaction (ORR) at platinum surface in an acidic electrolyte. In contrast to HOR at the anode, the cathode ORR is a highly irreversible reaction even at temperatures above 100 °C at the best existing catalyst – the platinum surface [16–19]. Gasteiger et al. [20] found that 0.4 mg Pt/cm^2 was close to the optimal platinum loading for the air electrode using the state-of-the-art Pt/C catalyst and an optimized electrode structure. Further reduction of the cathode platinum loading will result in cell voltage loss at low current densities that follows the ORR kinetic loss. The high platinum loading at the cathode originates from the slow kinetics of (ORR) at platinum surface. To make the fuel cell vehicles commercially viable on the market, the platinum loading on the cathode has to be reduced significantly. As shown in Fig. 1, when Pt loading requirement is translated from the target set for power-specific Pt consumption in g Pt/kW, a fourfold Pt mass activity (activity per unit platinum mass) improvement is required, if combined with a 50% reduction in mass transport-related voltage loss [21]. Recent increases in Pt prices suggest that one should be striving for at least an eightfold improvement.

There are two ways one might think of that could help to reach that goal: further increasing the platinum dispersion (defined as the ratio of surface metal atoms to total number of atoms) by making finer platinum particles, if there is no decrease of Pt-specific activity (activity per unit Pt surface area); or alternatively, increasing the Pt-specific activity. One could also seek a combination of these two approaches.

This selected brief review will be focused on the research and development progress on ORR kinetics. The origin of the problem related with the low ORR activity of platinum will be discussed, followed by a review of recent progress in making more active, more durable platinum-based ORR catalysts. These include platinum alloy catalysts, platinum monolayer catalysts, platinum nanowire and nanotube catalysts, and the more recent shape- and facet-controlled platinum-alloy nanocrystal catalysts. The progress in the mechanistic understanding on the correlation between the activity and the electronic and structural properties of surface platinum atoms will be reviewed as well. The future direction of the research on platinum-based catalysts for PEM fuel cell application will be proposed.

Electrocatalysis of the ORR at Platinum Surfaces

It is widely accepted that the ORR on platinum surfaces is dominantly a multistep and four-electron reduction process with H_2O being the final product. However, the detailed mechanism of ORR still remains elusive [17]. The overall four electron reduction of O_2 in acid aqueous solutions is

$$O_2 + 4H^+ + 4e^- \rightarrow 2H_2O;$$
$$E_0 = 1.229V \text{ vs NHE at } 298K$$

Since the four-electron reduction of oxygen is highly irreversible, the experimental verification of the thermodynamic reversible potential of this reaction is very difficult. The irreversibility of ORR imposes serious voltage loss in fuel cells. In most instances, the current densities practical for kinetic studies are much larger than the exchange current density of ORR; therefore the information obtained from current-potential data are confined only to the rate-determining step (RDS). On the other hand, in the ORR kinetic potential region, the electrode surface structure and properties strongly depend on the applied potential and the time held at that potential, which makes the reaction more complicated. While the relationship between the overall

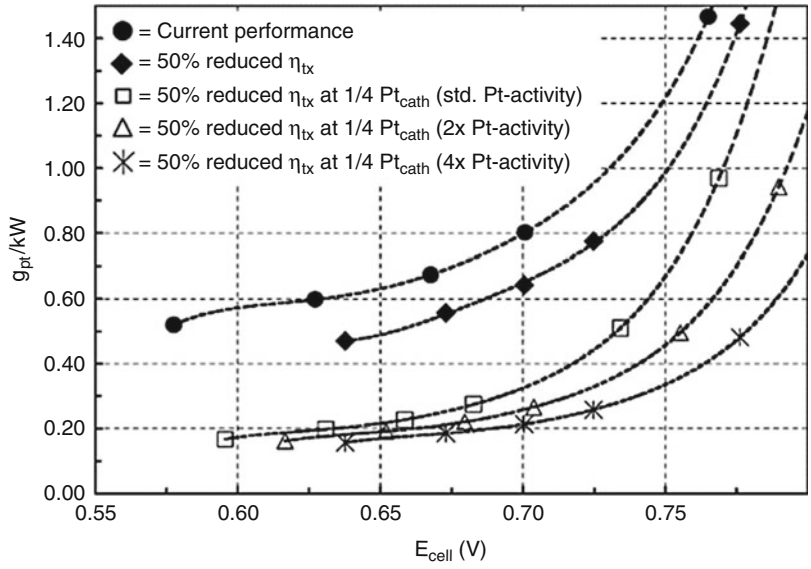

PEM Fuel Cells and Platinum-Based Electrocatalysts, Fig. 1 Pt-mass-specific power density [g_{Pt}/kW] versus cell voltage, E_{cell} [V], based on a 50 cm^2 single-cell H_2/air performance. η_{tx} = cell-voltage loss caused by mass transport; Pt_{cath} = cathode-Pt loading. The cell was tested at T_{cell} = 80°C, 100% RH (relative humidity), at a total pressure of 150 kPa_{abs} and stoichiometric flows of s = 2.0/2.0. Catalyst-coated membrane (CCM) was based on a ca. 25 25 μm low-EW (equivalent weight = 900) membrane, and ca. 50 wt% Pt/carbon (0.4/0.4 mg Pt/cm^2 (anode/cathode)). It was assumed that the cell performance could be maintained at a reduced anode loading of 0.05 mg Pt/cm^2 (Reproduced from [21] with permission)

kinetics and the surface electronic properties is not well understood, it is widely accepted that in the multistep reaction, the first electron transfer is the rate-determining step, which is accompanied by or followed by a fast proton transfer [16–18]. Two Tafel slopes are usually observed for ORR on Pt in RDE tests in perchloric acid, from −60 mV/decade at low current density, transitioning to −120 mV/decade at high current density. The lower Tafel slope of the ORR in perchloric acid at low current density has been attributed to the potential dependent Pt oxide/hydroxide coverage at high potentials [22–26].

Recently, by using Density Functional Theory (DFT), Norskov and coworkers [27] calculated the Gibbs free energy of ORR intermediates as a function of cathode potential based on a simple dissociative mechanism, i.e., with the adsorbed oxygen and hydroxide being the only intermediates. They found that oxygen or hydroxide is so strongly bound to the platinum surface at the thermodynamic equilibrium potential that proton and electron transfer become impossible. By lowering the potential, the stability of adsorbed oxygen decreases and the reaction may proceed. They suggested that these effects are the origin of the overpotential of the ORR on platinum surfaces.

By setting the reference zero potential to be NHE, the proton chemical potential in the electrolyte is related to the electrode potential. The authors made DFT calculations to get the bond energies of O* and HO* for a number of interesting metals. From this, they can evaluate the reaction free energies of the two basic steps: the hydrogenation of the two adsorbed intermediates O* and HO*. The larger one of the two reaction free energies was taken as the activation energy barrier of the rate-determining step (RDS) in ORR. By using a microkinetic model they constructed, the rate constant of the RDS, and therefore the ORR activity, can be evaluated based on the activation energy barrier. As shown in Fig. 2a, the model predicts a volcano-shaped relationship between the rate of the ORR and the oxygen adsorption energy, with platinum and

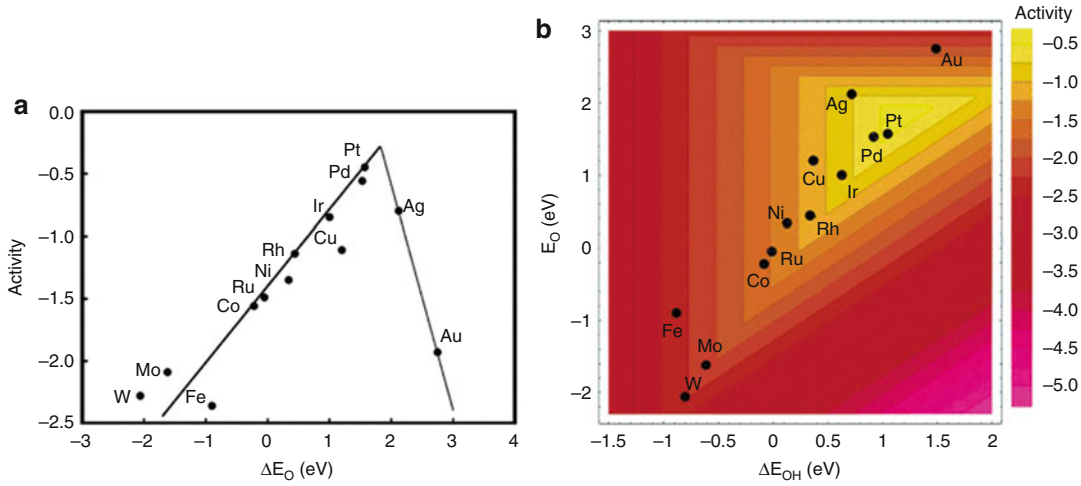

PEM Fuel Cells and Platinum-Based Electrocatalysts, Fig. 2 (**a**) Trends in oxygen reduction activity plotted as a function of the O-binding energy. (**b**) Trends in oxygen reduction activity plotted as a function of both the O and the OH-binding energy (Reproduced from [27]. With permission)

palladium being among the best metals for electrocatalysis of ORR. Fig. 2b shows that the bonding energy of OH is roughly linearly correlated to that of O, indicating both are nearly equivalent parameters in determining the ORR activity.

More recently, Wang et al. [28] derived an intrinsic kinetic equation for the four-electron ($4e^-$) oxygen reduction reaction (ORR) in acidic media, by using free energies of activation and adsorption as the kinetic parameters, which were obtained through fitting experimental ORR data from a Pt(111) rotating disk electrode (RDE). Their kinetic model consists of four essential elementary reactions: (1) a dissociative adsorption (DA); (2) a reductive adsorption (RA), which yields two reaction intermediates, O and OH; (3) a reductive transition (RT) from O to OH; and (4) a reductive desorption (RD) of OH, as shown below [28] (Reproduced with permission from [28]).

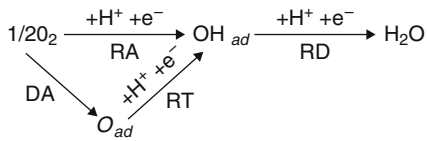

In contrast to a conventional ORR kinetic model, in this work there is no single particular RDS assumed, as the authors believe that a single RDS assumption may not hold over a wide potential region since the reaction pathway may change with potential, or there may exist two RDSs with similarly high activation barriers. The results indicate that the first electron transfer in the RA reaction ($\Delta G^{*0}_{\mathrm{RA}} = 0.46\mathrm{eV}$, where ΔG^{*0}_i is the activation energy of reaction i (at equilibrium potential)) is not the rate-determining step (RDS) for the ORR on Pt at high potentials, because dissociative adsorption ($\Delta G^{*0}_{\mathrm{DA}} = 0.26$ eV) provides a more active adsorption pathway. However, the reaction intermediates, O and OH, are strongly trapped on the Pt surface, requiring considerable overpotential to overcome the barriers for O to OH transition ($\Delta G^{*0}_{\mathrm{RT}} = 0.50\mathrm{eV}$) and OH reduction to water and desorption ($\Delta G^{*0}_{\mathrm{RD}} = 0.45\mathrm{eV}$).

Thus, the ORR on Pt is desorption-limited at high potentials, exhibiting a low apparent Tafel slope at those potentials. Wang et al. [29] further used this kinetic model to fit a typical IR-free polarization curve of a PEMFC, by adjusting the parameters to reflect the fuel cell-operating conditions at 80 °C. The results showed that the transition of the Tafel slope occurs at about the same 0.77 V that is the equilibrium potential for the transition between adsorbed O and OH on a Pt surface with low adsorbed O coverage [27].

Neyerlin et al. [30–32] investigated the ORR kinetics on high-surface-area carbon-supported platinum catalyst Pt/C in an operating PEMFC. By assuming the transfer coefficient $\alpha = 1$ and using a single Tafel slope, i.e., −70 mV/decade at 80 °C, three kinetic parameters could be extracted through fitting the kinetic model to the fuel cell data: the exchange current density or current density at a constant IR-free cell potential, the reaction order with respect to oxygen partial pressure, and the activation energy. One may need to note that the lower limit of the electrode potential after IR and transport correction in this work is about 0.77 V, so that this single-Tafel-slope treatment can still be consistent with Wang et al.'s [29] result. Neyerlin et al. [30] were concerned about the accuracy of the kinetic current extracted from low potentials in RDE tests, since at these low potentials the experimental measured current is more than ten times lower than the kinetic current derived from it. The transport correction used in RDE analysis assumes perfect first-order kinetics, which is not strictly true, and errors from this imperfect correction could become large at low potentials. The authors also studied the relative humidity (RH) effects on ORR kinetics in PEMFCs [32]. They found that when RH is above 50–60%, the kinetics are independent of the RH, but they observed significant ORR kinetic losses at lower RH. The reduction of ORR kinetics at low RH was interpreted as most likely due to a lowering of the proton activity (therefore only indirectly related to the lowering of the water activity) via hydration of acidic groups and the sequestering of protons at low RH.

Another factor that plays an important role in determining the minimum loading of Pt catalyst required for PEMFCs is the Pt size effect on ORR, not only through altering the fraction of surface Pt atoms over the number of total Pt atoms, but also through changing the ORR kinetics per surface Pt atom (Pt specific activity). Earlier results by Blurton et al. [33] showed that in 20% H_2SO_4 at 70 °C, the highly dispersed Pt (with size of about 1.4 nm) supported on conductive carbon prepared through ion exchange on resin followed by pyrolysis has a Pt-specific activity 20 times lower than that of crystalline Pt black (with size of about 10 nm), though it is not clear to what extend the lower activity could be caused by contamination of Pt and/or a "burying effect"during the catalyst preparation. Blurton et al. [33] correlated the decreased ORR specific activity with the decreased coordination number of surface Pt atoms on smaller Pt particles, causing more severe oxidation of the Pt surface. Peuckert et al. [34] later investigated a series of Pt-on-carbon catalysts with Pt weight percents from 5% to 30% prepared by an impregnation method, with corresponding fractions of metal atoms on the surface from 1.0 (Pt size <1 nm) to 0.09 (Pt size <12 nm). The Pt-specific activity toward ORR in 0.5 M H_2SO_4 at 298 K on these catalysts was found to be constant for Pt particle sizes above 4 nm but to decrease by a factor of 20 as the particle size decreased from 3 to 1 nm. Taking into account the larger percentage of buried and these inactive Pt atoms in larger particles, this result suggested that the optimal Pt size for the maximum Pt mass activity is about 3 nm. Kinoshita [35] also reviewed and analyzed the particle size effect for ORR on Pt/C catalysts. Based on the literature data of ORR on Pt/C collected in H_3PO_4 [36–38] and H_2SO_4 [34] solutions, Kinoshita proposed the decrease of Pt-specific activity with decrease of Pt particle size is a consequence of the changing distribution of surface atoms at the (100) and (111) crystal faces. Recent literature data [18] in H_3PO_4 reported that when Pt particle size increases from 2.5 to 12 nm, there is about threefold of increase in Pt-specific activity and confirmed the optimal Pt particle size for maximum mass activity to be around 3 nm. Gasteiger et al. [21] investigated Pt/C and Pt black catalysts for ORR in $HClO_4$ solution at 60 °C, with the Pt particle size ranging from 2 nm to over 10 nm, and found that the magnitude of activity improvement is comparable to that in literature data [39, 40], although the absolute values are about ten times higher than those reported in Ref. [40], due in part to the use of a less-strongly adsorbing electrolyte.

It is well established that ORR on Pt single crystals is structure-sensitive, depending on the electrolyte. In H_2SO_4, the order of activity of Pt(hkl) increases in the sequence (111)

<<(100) <(110) [19, 41]. The variation in H_2SO_4 originates from highly structure-specific adsorption of sulfate/bisulfate anions in this electrolyte, which has a strongly inhibiting effect on the (111) surface. Given that the dominant Pt crystal facets of high-surface-area Pt/C catalysts are {111} and {100}, the Pt size effect on ORR activity in H_2SO_4 can be explained by the structure-sensitive adsorption. In perchloric acid, the variation in activity at is relatively small between the three low index faces, with activity increasing in the order (100) < (111) (110) [42], owing to the structure sensitive inhibiting effect of OH_{ads}, i.e., a stronger inhibiting effect on (100) and smaller effects on (110) and (111) [41]. Norskov and other researchers [43–48], based on their DFT calculations, recently proposed using the concept of averaged d-band center energy to explain the reactivity of metal surface atoms, which was supported by numerous experimental data. According to them, when Pt particle size decreases, the average coordination number of surface Pt atoms decreases, causing the d-band center to move closer to the Fermi level and the reactivity of those atoms to increase. As a result of that, the Pt atoms bind oxygen-hydroxide stronger, and therefore, have a lower ORR activity. A stronger adsorption of OH species on Pt surface when the particle size is reduced to below 5 nm was reported in Ref. [49].

While the Pt particle-size effect on ORR suggests that a further increase of Pt dispersion by decreasing the particle size to much smaller than 3 nm will not improve Pt mass activity, it is worth noting that the Pt-size effect is not universally believed. Recently, Yano et al. [50] studied ORR on a series of carbon-supported Pt-nanoparticle electrocatalysts (Pt/C) with average diameters in the range of roughly 1–5 nm, combined with measurements on ^{195}Pt electrochemical nuclear magnetic resonance (EC-NMR) spectroscopy. They observed that ORR rate constants and H_2O_2 yields evaluated from hydrodynamic voltammograms measurements did not show any particle size dependency. The apparent activation energy of 37 kJ mol^{-1}, obtained for the ORR rate constant, was found to be identical to that obtained for bulk platinum electrodes. This was consistent with the negligible difference in the surface electronic properties of these Pt/C catalysts, revealed from the practically no change of surface peak position of ^{195}Pt NMR spectra and the spin-lattice relaxation time of surface platinum atoms with the particle size variation.

Nevertheless, facilitating the ORR kinetics by augmenting the Pt specific activity is important for the future of fuel cells. A recent perspective in *Science* by Gasteiger and Markovic [51] showed some promising advances in this aspect.

Pt-Alloy Electrocatalysts

Pt-alloy catalysts, predominantly Pt binary and ternary alloys with 3D transition metals, have been the main focus of catalyst research for PEM fuel cells in the past decades, as they confer enhanced ORR activities over those available from pure Pt catalysts. Great progress has been made in past decades in developing more active and durable Pt alloy catalysts and in understanding the mechanism of their activity enhancements. Two- to threefold specific activity enhancements versus pure Pt were typically reported in literature [21, 40, 52–54], while exceptions existed from earlier results, claiming either no enhancement [55–57], or over an order of magnitude enhancement [58]. As far as which alloy and what alloy compositions confer the highest ORR activity, there seems to be lack of general agreement. This is probably because the measured activity depends highly on the catalyst surface and near-surface atomic composition and structure, on impurities on the surface, and on particle size and shape, all of which could be affected by the preparation method, heat treatment protocol, and testing conditions. For example, to achieve the optimal alloy structure for maximum activity, different Pt alloy particles may require different annealing-temperature protocols to accommodate the distinctions between metal melting points and particle sizes [59, 60]. In a number of earlier papers [61–63] it was showed that Pt-Cr is the most active ORR cathode catalyst in phosphoric acid fuel cells, while some recent results reported that in the PEMFC-oriented settings, the most

active Pt alloy ORR catalyst could be Pt-Co [64], Pt-Fe [58, 65], Pt-Cr [52], Pt-Ni [66], or Pt-Cu [67] at specific atomic ratios of Pt to the alloying elements. Several representative mechanisms have been proposed in the literature to explain the enhanced activities observed on Pt alloy catalysts: (1) a surface roughening effect due to leaching of the alloy base metal [68, 69]; (2) decreased lattice spacing of Pt atoms due to alloying [52, 61, 70];(3) electronic effects of the neighboring atoms on Pt, such as increased Pt d-band vacancy [52, 58, 65, 71] or depressed d-band center energy upon alloying [42, 64, 67, 72, 73]; and/or (4) decreased Pt oxide/hydroxide formation at high potential [52, 74–76]. The increased Pt surface roughness alone may help increase Pt mass activity but will not increase the Pt-specific activity. Other mechanisms are correlated with each other, for example, the decreased lattice spacing may affect the electronic structure of Pt atoms, which in turn may inhibit the Pt oxide/hydroxide formation. A more detailed discussion follows.

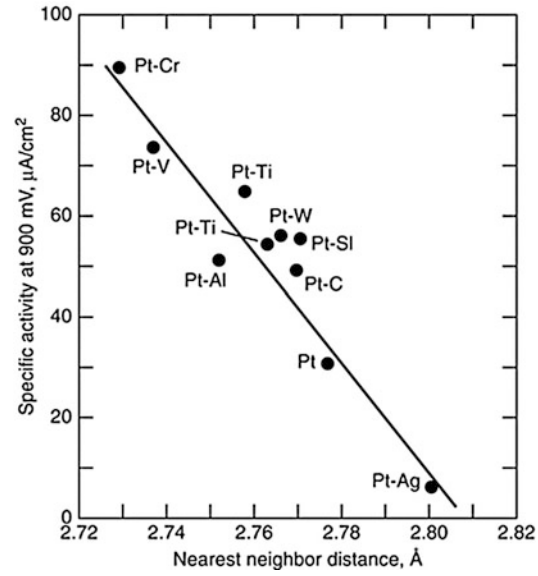

PEM Fuel Cells and Platinum-Based Electrocatalysts, Fig. 3 Specific activity for the ORR versus electrocatalyst nearest-neighbor distance (Reproduced from [61] with permission)

Jalan and Taloy [61] believed that the nearest-neighbor distance between Pt atoms plays an important role in the ORR, based on the reaction model proposed by Yeager et al. [16], i.e., the rate-determining step being the rupture of O-O bond via various dual site mechanisms. They proposed that the distance between nearest-neighbor atoms on the surface of pure Pt is not ideal for dual site adsorption of O_2 or "HO_2" and that the introduction of foreign atoms that reduce the Pt nearest-neighbor spacing would result in higher ORR activity. By testing a number of carbon-supported Pt-M alloy catalysts fabricated into gas diffusion electrodes, with various nearest-neighbor Pt atom distances determined from X-ray diffraction, a linear relationship was obtained between the activity and the distance, with Pt-Cr exhibiting highest ORR activity and smallest nearest-neighbor distance, as shown in Fig. 3. While the geometric distance between the neighboring Pt atoms is shorter in alloys, the surface electronic structure of Pt alloys is different from that of pure Pt as well, so it is difficult to separate the two factors. Yet other studies [55, 68, 69] claimed no activity enhancement was observed on Pt-Cr alloy over pure Pt, except for the increased surface roughness [68, 69], but this has not been supported by more recent literature [52, 70].

Mukerjee and coworkers did a series of studies [52, 74, 77, 78] on Pt binary alloys for ORR applying in situ X-ray absorption spectroscopy (XAS) to electrochemical systems. The spectra consist of two parts, the near-edge part XANES (X-ray absorption near-edge structure), which gives chemical information and EXAFS (extended X-ray absorption fine structure), which gives the structural information around the element of interest. In a related study, Mukerjee et al. [52] investigated five binary Pt alloys (PtCr/C, PtMn/C, PtFe/C, PtCo/C, and PtNi/C) supported on high-surface-area carbon for ORR in a proton exchange membrane fuel cell. The electrode kinetic studies on the Pt alloys showed a two- to threefold increase in ORR activity relative to a reference Pt/C electrocatalyst, with the PtCr/C alloy exhibiting the best performance. Contractions in the Pt-Pt bond distances were observed by both EXAFS and XRD. In addition, they found that in the double-layer potential region (0.54 V versus RHE), the alloys possess

higher Pt d-band vacancies than Pt/C, while in the high potential region (0.84 V versus RHE), Pt/C shows higher d-band vacancy relative to alloys. This was interpreted by the adsorption of OH species at high potential on Pt/C but to a lesser extent on Pt alloys. Correlation of the electronic (Pt d-band vacancies) and geometric (Pt-Pt bond distance) with the electrochemical performance characteristics exhibits a volcano-type behavior with the PtCr/C alloy being at the top of the curve, shown in Fig. 4. They rationalized the enhanced activity on alloys on the basis of electronic and geometric effects, and of inhibition of OH adsorption. Similar observations were also reported from the ORR measurements in phosphoric acid [66], and in alkaline solution [79–81].

Surface segregation of Pt has been experimentally observed in a wide range of Pt-M binary alloys, such as Pt-Fe [82], Pt-Ni [83], Pt-Co [84], Pt-Ru [85], and has also been reported in theoretical calculations [86, 87]. Furthermore, it has been reported that the topmost layer is composed of pure Pt while the second layer is enriched in the transition metal M for Pt-rich Fe, Co, and Ni alloys [72, 76, 88], produced by displacement of Pt and M atoms in the first two layers to minimize the surface free energy during annealing. Stamenkovic et al. [76] studied polycrystalline Pt_3Ni and Pt_3Co alloys for electrocatalysis of ORR in acid electrolytes using the rotating ring disk electrode (RRDE) method. Polycrystalline bulk alloys of Pt_3Ni and Pt_3Co were prepared in ultra-high vacuum (UHV) having two different surface compositions: one with 75% Pt (by sputtering) and the other with 100% Pt (by annealing). The latter was called a "Pt-skin" structure and is produced by an exchange of Pt and Co in the first two layers. Activities of Pt-alloys for the ORR were compared to those of polycrystalline Pt in 0.5 M H_2SO_4 and 0.1 M $HClO_4$ electrolytes. It was found that in H_2SO_4, the activity increased in the order $Pt_3Ni > Pt_3Co >$ Pt; in $HClO_4$, however, the order of activities was "Pt-skin/Pt_3Co" > Pt_3Co > Pt_3Ni > Pt. The catalytic enhancement was greater in 0.1 M HClO4 than in 0.5 M H_2SO_4, with the maximum enhancement observed for the "Pt-skin" on Pt_3Co in 0.1 M $HClO_4$ being three to four times

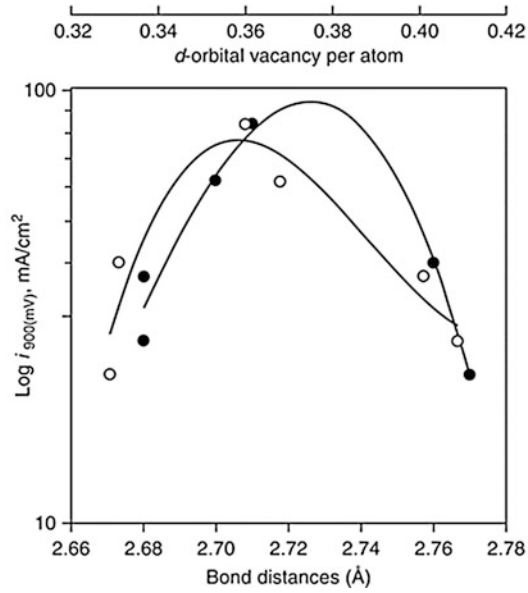

PEM Fuel Cells and Platinum-Based Electrocatalysts, Fig. 4 Correlation of the ORR performance of Pt and Pt-alloy electrocatalysts in PEMFC with Pt-Pt bond distance (*solid circles*) and the d-band vacancy of Pt (*empty circles*) obtained from in situ XAS (Reproduced from [52] with permission)

that for pure Pt. The activity enhancement was attributed to the inhibited Pt-OH_{ad} formation on an alloy, even one covered with pure Pt, relative to the surface of a pure-Pt electrode, and the ORR reaction mechanism (pathway) was found to be the same on alloys as on a pure-Pt electrode. In a more recent study, Stamenkovic et al. [64] investigated polycrystalline Pt_3M (M = Ni, Co, Fe, Ti, V) surfaces for ORR in 0.1 M $HClO_4$, for both "Pt-skin" and sputtered alloy surfaces. The activity was correlated to the d-band center energy obtained in UHV via ultraviolet photoemission spectroscopy (UPS). A "volcano behavior" was revealed with the Pt_3Co has the highest activity for both "Pt-skin" and sputtered surfaces. The "Pt-skin" surface was found to be more active than sputtered surface again for each Pt_3M. The electrochemical and post-electrochemical UHV (ultra-high vacuum) surface characterizations revealed that Pt-skin surfaces are stable during and after immersion to an electrolyte. In contrast, all sputtered surfaces formed Pt-skeleton

outermost layers due to dissolution of transition metal atoms [89].

By using DFT calculations, Xu et al. [47] studied the adsorption of O and O_2 and the dissociation of O_2 on the (111) faces of ordered Pt_3Co and Pt_3Fe alloys and on monolayer Pt skins covering these two alloys. Results were compared with those calculated for two Pt(111) surfaces, one at the equilibrium lattice constant and the other laterally compressed by 2% to match the strain in the Pt alloys. The absolute magnitudes of the binding energies of O and O_2 follow the same order in the two alloy systems: Pt skin < compressed Pt(111) < Pt(111) < Pt_3Co(111) or Pt_3Fe(111). The reduced bonding strength of the compressed Pt(111) and Pt skins for oxygen was rationalized as being due to the shifting of the d-band center increasingly away from the Fermi level. They proposed that an alleviation of poisoning by O and enhanced rates for reactions involving O could be some of the reasons why Pt skins are more active for the ORR.

Chen et al. [88, 90] recently studied carbon supported Pt_3Co nanoparticles for ORR and correlated their activity with the chemical composition and structural information of individual particles. Conventional and aberration-corrected high-angle annular dark-field (HAADF), scanning transmission electron microscopy (STEM), and high resolution transmission electron microscopy (HRTEM) were used to obtain the particle compositional and structural information. For the acid treated Pt_3Co nanoparticles, they observed the formation of percolated Pt-rich and Pt poor regions within individual nanoparticles, analogous to the skeleton structure observed for sputtered polycrystalline Pt alloy surfaces after acid leaching [89]. The acid treated alloy nanoparticles yielded about two times the specific activity of pure-Pt nanoparticles. After annealing of the acid-treated particles, sandwich-segregation surfaces of ordered Pt_3Co nanoparticles were directly observed, with the topmost layer being pure Pt atoms. The specific activity of annealed nanoparticles was about four times that of pure Pt nanoparticles. The enhanced Pt-specific activity toward ORR was attributed to the reduced binding energy of oxygenated species, owing to combined two effects, i.e., the increased compressive strain in Pt atoms, and the ligand effect from underlying Co atoms.

Strasser et al. [59, 67, 91–94] recently applied a freeze-drying technique in the synthesis of Pt alloy nanoparticle catalysts with enhanced ORR activity. The Pt-Cu alloy catalyst after electrochemical dealloying was reported to have both mass and specific activities about four to six times those of a standard commercial Pt/C catalyst, in both RDE and MEA tests. The synthesis involved an impregnation/freeze-drying route followed by annealing. Preparation started with impregnation and sonication of a commercial 30 wt% Pt/C catalyst with an aqueous solution of a copper nitrate, with Pt:Cu atomic ratio of 1:3, followed by freezing in liquid N_2. The frozen sample was subsequently freeze-dried under a moderate vacuum (0.055 mbar). Reduction and alloying of Pt and Cu on the carbon support was thermally driven under a reductive H_2 atmosphere in a tube furnace. Electrochemical etching (voltammetric dealloying) was employed to remove the surface Cu atoms from Cu-rich Pt-Cu alloy precursors. Bulk and surface structural and compositional characterization suggested that the dealloyed active catalyst phase consists of a core-shell structure in which a multilayer Pt rich shell is surrounding a Pt-poor alloy particle core. This work constitutes significant progress on initial activity, since a fourfold of increase of Pt mass activity is the performance target for commercially viable fuel cell cathode catalyst [21]. Fig. 5a shows a schematic of the dealloying process, and Fig. 5b exhibits the Pt mass activities of Pt-Cu/C synthesized at different temperatures, compared with the Pt/C catalyst.

As to the mechanistic origin of the activity enhancement in dealloyed Pt-Cu catalyst, the authors believe geometric effects play a key role, because the low residual Cu near-surface concentrations make significant electronic interactions between Pt and Cu surface atoms unlikely. Therefore, they suspect that the dealloying creates favorable structural arrangements of Pt atoms at the particle surface, such as more active crystallographic facets or more favorable Pt-Pt interatomic distances for the electroreduction of oxygen, as

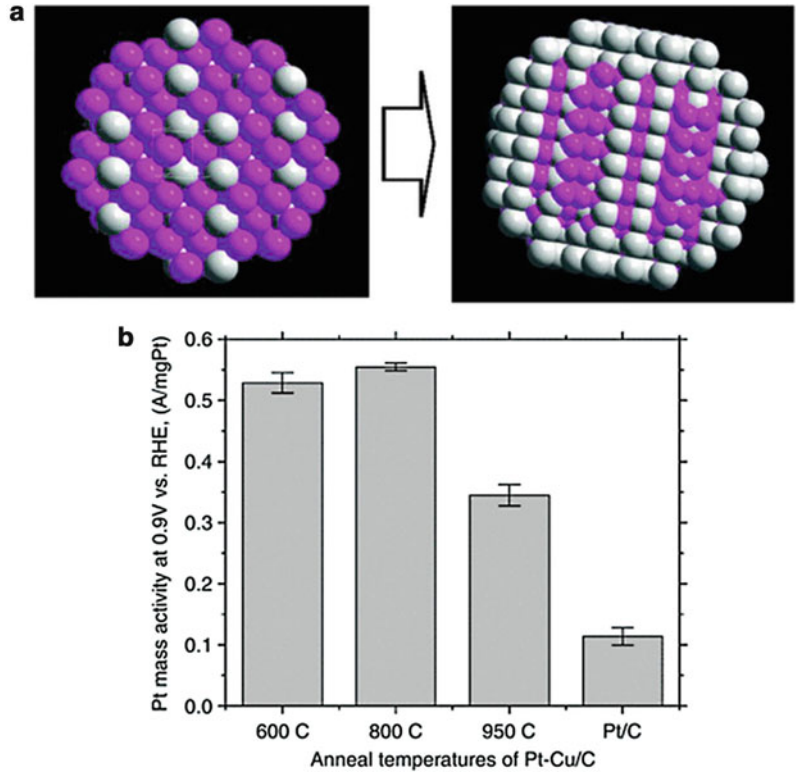

PEM Fuel Cells and Platinum-Based Electrocatalysts, Fig. 5 (**a**) The schematic model of a Pt-Cu alloy particle before and after electrochemical dealloying of the near-surface Cu atoms (*pink balls* = Cu atoms; *gray balls* = Pt atoms); (**b**) Pt mass activities of Pt-Cu/C catalysts at various annealing temperatures compared to that of Pt/C catalyst (Reproduced from [67] with permission)

predicted by DFT calculations [47]. A fourfold enhancement in Pt mass activity on monodispersed Pt_3Co nanoparticles with particle size of 4.5 nm was also reported recently [95].

Watanabe and coworkers carried out a series of studies on the mechanism for the enhancement of ORR activity on Pt-Fe, Pt-Ni, and Pt-Co alloys [53, 58, 65, 71, 96, 97]. By using X-ray photoelectron spectroscopy combined with an electrochemical cell (EC-XPS) [96, 97], they identified quantitatively oxygen-containing species adsorbed on electrodes of a pure Pt and a Pt skin layer (generated by acid treatment, not annealing, and therefore equivalent to the "skeleton" layers described by Stamenkovic et al. [89]) formed on Pt-Fe and Pt-Co alloys' surface from N_2- and O_2-saturated 0.1 M HF solution. Four types of species were distinguished with binding energies at 529.6, 530.5, 531.1, and 532.6 eV; the first two were assigned to O_{ad} and OH_{ad}, while the latter two were assigned to the bilayer water molecules, $H_2O_{ad,1}$ and $H_2O_{ad,2}$. The XPS results showed that the Pt skin layer exhibited a higher affinity to O_{ad} but less to H_2O compared to pure Pt, particularly in the O_2-saturated solution. The enhanced ORR activity at the Pt skin/Pt-alloy electrode was ascribed to higher coverage of O_{ad} than that at pure Pt. They also found that such an enhancement is induced without changing the activation energy but the corresponding frequency factor value in the pre-exponential term from that of pure Pt. From the measurements in a flow channel with 0.1 M $HClO_4$, in the temperature range of 20–50 °C, a two to fourfold of ORR-specific activity enhancement was reported for those Pt alloys [53].

Pt metal dissolution in fuel cells has been reported to play a key role in Pt surface area loss and cell performance loss [98]. While Pt-alloy catalysts with fourfold enhancement in both Pt mass activity and specific activity relative to standard Pt/C catalyst seem achievable, as has been shown above, the long-term durability of the alloy catalysts is still a concern, due to dissolution of the base metal from the alloys [21, 99]. For Pt-Cu alloy catalysts, an additional possible risk is that

the dissolved Cu may migrate from cathode through membrane to anode and deposit on the anode Pt surface, causing a poisoning effect on anode hydrogen oxidation kinetics, as the Cu redox potential is higher than the anode hydrogen redox potential. Fortunately, the durability of the cathode catalyst can be compensated by careful system control, mainly through lowering the cathode upper potential limit and narrowing its operating potential window [100, 101].

Pt Monolayer Electrocatalysts

Pioneered by Adzic et al. [102, 103], the idea of a Pt monolayer electrocatalyst has been one of the key concepts in reducing the Pt loading of PEM fuel cells in recent years. Pt submonolayers deposited on Ru nanoparticles had been earlier demonstrated to give superior performance with ultralow Pt loading compared to commercial Pt/C or Pt-Ru alloy catalysts for the anode CO-tolerant hydrogen oxidation reaction [103–107]. More recently, Adzic and coworkers applied this concept in making novel Pt monolayer catalysts for the cathode ORR, which will be the focus of the review in this section. In general, the new method of synthesizing Pt monolayer catalysts involves underpotential deposition (UPD), a technique well known to produce an ordered atomic monolayer to multilayer metal deposition onto a foreign metal substrate [108–110]. Specifically, the method consists of two steps [111, 112]: first, a monolayer of a sacrificial less-noble metal is deposited on a more noble metal substrate by UPD, such as Cu UPD on Au or Pd; second, the sacrificial metal is spontaneously and irreversibly oxidized and dissolved by a noble metal cation, such as a Pt cation, which is simultaneously reduced and deposited onto the foreign metal substrate. The whole procedure can be repeated in order to deposit multilayers of Pt (or another noble metal) on the foreign metal.

The advantages of Pt monolayer catalysts include (1) full utilization of the Pt atoms that are all on the surface, and (2) that the Pt activity and stability can be tailored by the selection of the substrate metals. For example [102], when a Pt monolayer is deposited onto different substrate metals, as shown in Fig. 6, due to the lattice mismatch between the metals, it can experience compressive or tensile stress, which is known to affect the Pt activity by adjusting its d-band center energy [43, 47] and consequently its ORR activity.

Pt monolayer deposits on Pd(111) single crystals (Pt/Pd(111)) and on Pd/C nanoparticles (Pt/Pd/C) have been studied for ORR [112], and improved activities compared to Pt(111) and commercial Pt/C, respectively, were reported. The ORR reaction mechanism of the monolayer catalysts was found to be the same as that on pure Pt surface. Pt/Pd(111) was found to have a 20 mV improvement in half-wave potential versus Pt (111), and the Pt/Pd/C had a Pt-mass activity five- to eight-times higher than that of Pt/C catalyst. If the total noble metal amount (Pt + Pd) is counted, the mass activity is about 80% higher than that of Pt/C catalyst [112]. The enhanced ORR activity is attributed to the inhibited OH formation at high potential, as evidenced from XAS measurements. In a real fuel cell test, 0.47 g Pt/kW was demonstrated at 0.602 V [113].

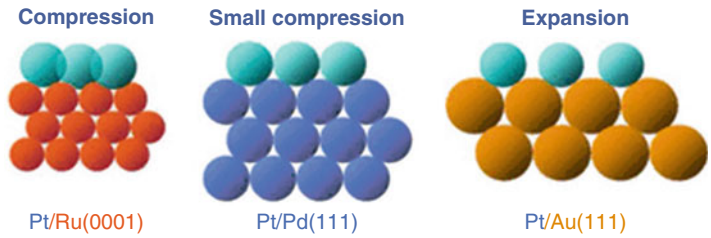

PEM Fuel Cells and Platinum-Based Electrocatalysts, Fig. 6 Models of pseudomorphic monolayers of Pt on three different substrates inducing compressive strain (Ru (0001) and Pd(111)) and tensile strain (Au(111)). (Reproduced from [102] with permission)

In order to understand the mechanism for the enhanced activity of a Pt monolayer deposited on Pd metal, the ORR was investigated in O_2-saturated 0.1 M $HClO_4$ solution on platinum monolayers supported on Au(111), Ir(111), Pd (111), Rh(111), and Ru(0001) single-crystal RDE surfaces [114]. A comparison of the polarization curves at 1600 rpm is shown as in Fig. 7. The trend of the ORR activities increase in the sequence Pt/Ru(0001) < Pt/Ir(111) < Pt/Rh (111) < Pt/Au(111) < Pt(111) < Pt/Pd(111).

The authors further correlated the kinetic activities of the "monolayers" with the Pt d-band center energies (not shown) and Pt-O binding energies, and found a "volcano" relationship, with the Pt/Pd (111) having the optimal d-band center, as well as Pt_{ML}-O-binding energy, for the maximum ORR activity. The "volcano" behavior was rationalized as being controlled by the two key steps in ORR, the O-O bond dissociation which is followed by the other step, the O-H bond formation. As shown in Fig. 8, the activation energies of the two steps both correlated linearly with the Pt_{ML}-O-binding energies (and with the d-band center energies, not shown), but in the opposite trend, indicating the Pt_{ML}-O binding can be neither too strong, nor too weak, for the best ORR activity.

For further fine-tuning of the monolayer Pt/Pd ORR activity, they further introduced mixed metal + Pt monolayer catalysts [115], which contained

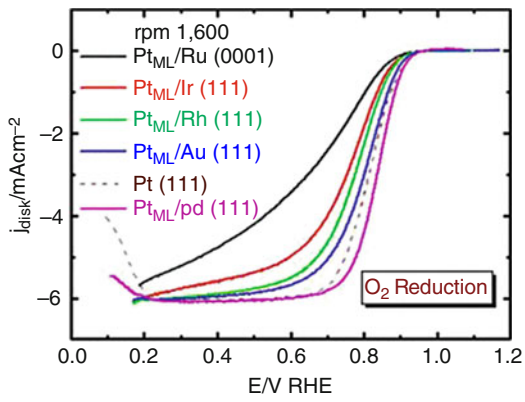

PEM Fuel Cells and Platinum-Based Electrocatalysts, Fig. 7 Polarization curves for O_2 reduction on platinum monolayers in 0.1 M $HClO_4$ solution on a RDE. Rotation rate = 1,600 rpm (Reproduced from [114] with permission)

0.2 monolayer of a foreign metal from selection of (Au, Pd, Rh, Ir, Ru, Os, and Re) combined with 0.8 monolayer of Pt co-deposited on Pd(111) or on Pd/C nanoparticles. The foreign metals have either a weaker M-OH bond (for the case of Au-OH), or a stronger M-OH bond (for the rest of the cases) than the Pt-OH bond. DFT calculations [115] showed that, in addition to altering the Pt d-band center energies, the $OH_{(-M)} - OH_{(-Pt)}$ (or $O_{(-M)} - OH_{(-Pt)}$) repulsion plays an important role in augmenting the ORR activity, as shown below in Fig. 9. Instead of adjusting the composition of the top2most Pt monolayer, replacing the substrate Pd(111) with $Pd_3Fe(111)$ to generate $Pt/Pd_3Fe(111)$ was recently reported to also have an enhanced ORR activity [116].

Another type of Pt monolayer catalyst showing improved ORR activities are Pt monolayers deposited on (noble metal)/(non-noble metal) core-shell nanoparticles [117]. The synthesis approach started with impregnation of high surface carbon into a mixed solution of noble metal precursor and non-noble metal precursor, followed by stir-drying in air. Core-shell metal substrates were formed by surface segregation of the noble metal at elevated temperature in a reductive atmosphere. A Pt monolayer was then deposited on the core/shell substrates by galvanic displacement of a Cu monolayer that was UPD-deposited onto the core-shell substrate particles. Three combinations were investigated: Pt/Au/Ni, Pt/Pd/Co, and Pt/Pt/Co. The enhancement of Pt mass activity of the best case (Pt/Au/Ni) was reported as being over an order of magnitude relative to the commercial Pt/C catalyst. The total noble metal mass activities were reported to be 2.5–4 times higher than that of Pt/C, with the Pt/Pt/Co having the highest number. The enhancement of activities was attributed to the geometric effect induced by the fine-tuning of the Pt lattice spacing with the substrate core-shell particles and to the inhibited PtOH formation because of lowering of the d-band center position relative to the Fermi level.

In a related study, Zhang et al. [118] investigated a partial monolayer of Au deposited on Pt (111) and on Pt/C nanoparticles for ORR. The catalysts were synthesized by Au displacement

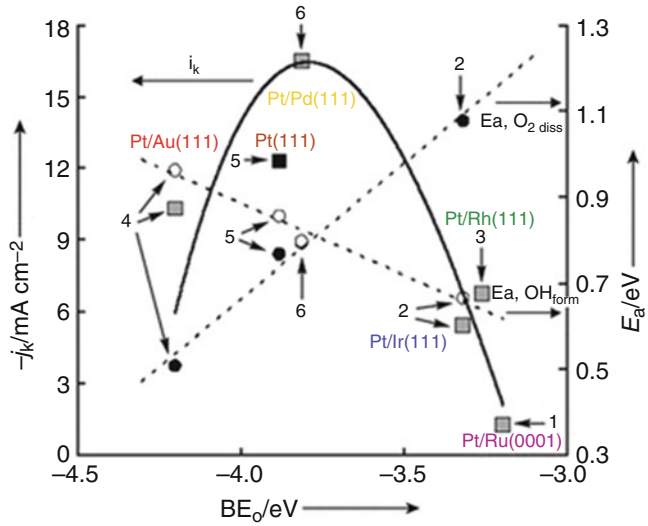

PEM Fuel Cells and Platinum-Based Electrocatalysts, Fig. 8 Kinetic currents (j_K; *square symbols*) at 0.8 V (versus RHE) calculated from Fig. 7 for ORR and the activation energies for O_2 dissociation (*solid circles*) and for OH formation (*empty circles*) on Pt/Ru(0001) (1); Pt/Ir (111) (2), Pt/Rh(111) (3), Pt/Au(111) (4), Pt(111) (5) and Pt/Pd(111) (6), as functions of the calculated binding energy of atomic oxygen (BEO) (Reproduced from [114] with permission)

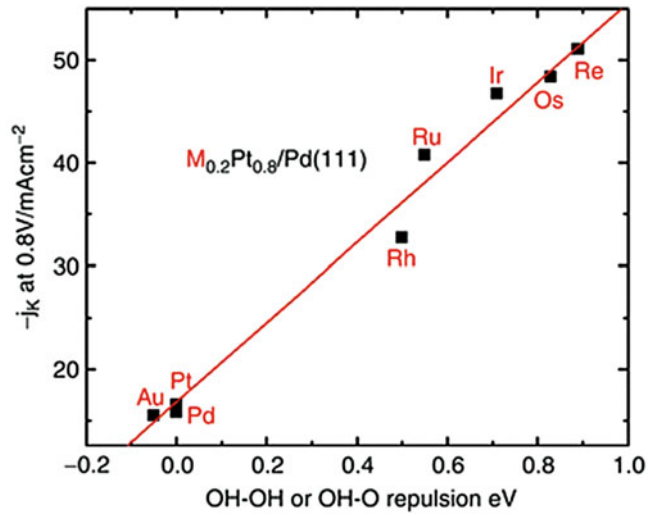

PEM Fuel Cells and Platinum-Based Electrocatalysts, Fig. 9 Kinetic current at 0.80 V as a function of the calculated interaction energy between two OHs, or OH and O. Positive energies indicate more repulsive interaction compared to Pt/Pd(111) (Reproduced from [115] with permission)

of a monolayer Cu that was deposited with UPD onto the Pt(111) or Pt/C substrates. Due to the valence-state difference between Au^{3+} and Cu^{2+}, two thirds of a monolayer of Au was deposited onto each of the Pt surfaces. The Au atoms appeared to form clusters on Pt surfaces. While the ORR activities of the Au/Pt(111) and Au/Pt/C catalysts were slightly lower than those of pure Pt (111) and Pt/C catalysts, respectively; the stability of the Au/Pt/C was superior compared to that of Pt/C catalyst. Potential cycling tests were performed on RDE in 0.1 M $HClO_4$ solution, with the potential cycling window between 0.6 and 1.1 V, for 30,000 cycles. The catalytic activity of Au/Pt/C, measured as half-wave potentials on the O_2 reduction polarization curves obtained

before and after potential cycling, showed only a 5 mV degradation in over the cycling period. In contrast, the corresponding change for Pt/C amounted to a loss of 39 mV. In situ X-ray absorption near-edge spectroscopy (XANES) with respect to the potential applied on the catalyst surfaces revealed the oxidation of Pt nanoparticles covered by Au at high potentials was decreased in comparison with the oxidation of Pt nanoparticles lacking such coverage.

More recently, Wang et al. [119] investigated the ORR on well-defined Pt/Pd and Pt/PdCo core-shell nanoparticles for the effects of particle size, facet orientation, and Pt shell thickness. The Pt shell was generated and the shell thickness was controlled by a novel method called the Cu-UPD-mediated electrodeposition method, in which repeated Cu-UPD/stripping, potential cycling, and Pt irreversible deposition occurred simultaneously in the same electrolyte, with the Pt deposition under diffusion control, until a desired thickness of Pt was achieved. Atomic level analysis using Z-contrast scanning transmission electron microscopy (STEM) coupled with element-sensitive electron energy loss spectroscopy (EELS) showed that well-controlled core-shell particles were obtained. ORR tests on RDE showed that Pt-monolayer catalysts on 4 nm Pd and 4.6 nm Pd_3Co cores exhibited 1.0 and 1.6 A/mg Pt mass activities at 0.9 V, respectively, about five- and ninefold enhancements over that of 3 nm Pt nanoparticles. Also, two- and threefold enhancements in specific activity were observed respectively, which were mainly attributed to the nanosize- and lattice-mismatch-induced contraction in (111) facets based on the DFT calculations using a nanoparticle model. Scale-up methods were developed for synthesis of the core-shell particles [120].

In summary, Pt monolayer catalysts show a promising pathway toward solving one of the major problems facing PEM fuel cells by enhancing the Pt-specific activity and the utilization of Pt atoms, and therefore reducing the cost of the cathode catalyst, although more fuel cell tests of durability are needed before the monolayer catalysts can be put in fuel cell vehicles. There is still a need for a reduction in the total noble metals in these catalysts.

Pt and Pt-Alloy Nanowire and Nanotube Electrocatalysts

As has been discussed in the introduction, low activity and limited durability are the two major issues related to the high-surface-area-carbon-dispersed Pt nanoparticle catalysts (Pt/C) in PEM fuel cells. Shao-Horn et al. [121] have given a comprehensive review on the instability considerations of Pt/C catalysts. Conventional PEM fuel cell catalysts typically consist of Pt nanoparticles in size of 2–3 nm that are supported on high-surface carbon with 20–50 nm primary carbon particles for electrical conductivity and high levels of catalyst activity. As it has been shown above, this kind of catalyst has already approached the maximum Pt mass activity as a pure Pt/C catalyst, as the Pt particle size is close to the optimal value. However, the 2–3 nm Pt nanoparticles are intrinsically not stable enough under PEM fuel cell operating conditions if no system-mitigation methods are applied. As an example, for a fuel cell short stack operating at steady-state open-circuit voltage (OCV, <0.95 V versus RHE), with H_2/air flows (stoichiometric reactant flows of $s = 2/2$) at 80 °C, fully humidified and 150 kPa_{abs} for 2000 h, the Pt surface area decreased from <70 m^2/g Pt to <15 m^2/g Pt, corresponding to an almost 80% of Pt surface area loss [98]. If accompanied by a similar percentage loss of activity, this is not acceptable for commercialization of fuel cell vehicles. In addition, corrosion of carbon support makes the situation even more serious [122, 123]. One way to address this issue is to lower the upper voltage limit of the fuel cell through system mitigation [100, 101], or alternatively, to improve the intrinsic Pt stability through catalyst design, such as using Pt or Pt-alloy nanowire/nanotube catalysts. The local curvature of the nanowire/nanotube Pt or its alloy is expected to be small (in at least one direction), and it consequently has a lower surface free energy and higher stability. On the other hand, the Pt-specific activity of the nanowire/nanotube is expected to be higher than its nanoparticle counterpart, as it should bind OH/O less strongly.

The 3M nanostructured thin film (NSTF) catalyst is such a non-conventional catalyst [124, 125]. The support particle is a crystalline organic pigment material, perylene red (PR), which is vacuum-deposited and converted to an oriented whisker phase by thermal annealing. The result is a uniquely structured thin film composed of highly oriented, densely packed crystalline organic whiskers [126]. A crystalline Pt coating can be vacuum-deposited on the whiskers. Fig. 10 shows SEM images of the NSTF catalyst-coated whiskers prior to incorporation onto the surfaces of a PEM to form a catalyst-coated membrane [127]. The cross section of the whiskers is on the order of 50 nm, and the lengths of the whiskers are controllable by the thickness of the as-deposited PR film, typically in the range of 0.5–2 μm. For a practical loading of <0.2 mg Pt/cm^2, the typical Pt crystallite size of the coated PR whiskers is 10–11 nm, and the specific surface areas of the NSTF-Pt catalysts are <10 m^2/g Pt [124].

Bonakdarpour et al. [128] investigated Pt/NSTF and Pt-Co-Mn/NSTF for ORR by using the rotating ring disk electrode (RRDE). The nominal chemical composition of the ternary alloy was calculated to be $Pt_{0.68}Co_{0.3}Mn_{0.02}$. The catalyst-coated whiskers were carefully brushed off of the original substrate web and applied onto the glassy carbon disk of the RRDE. The measurements were done in O_2-saturated 0.1 M $HClO_4$ at room

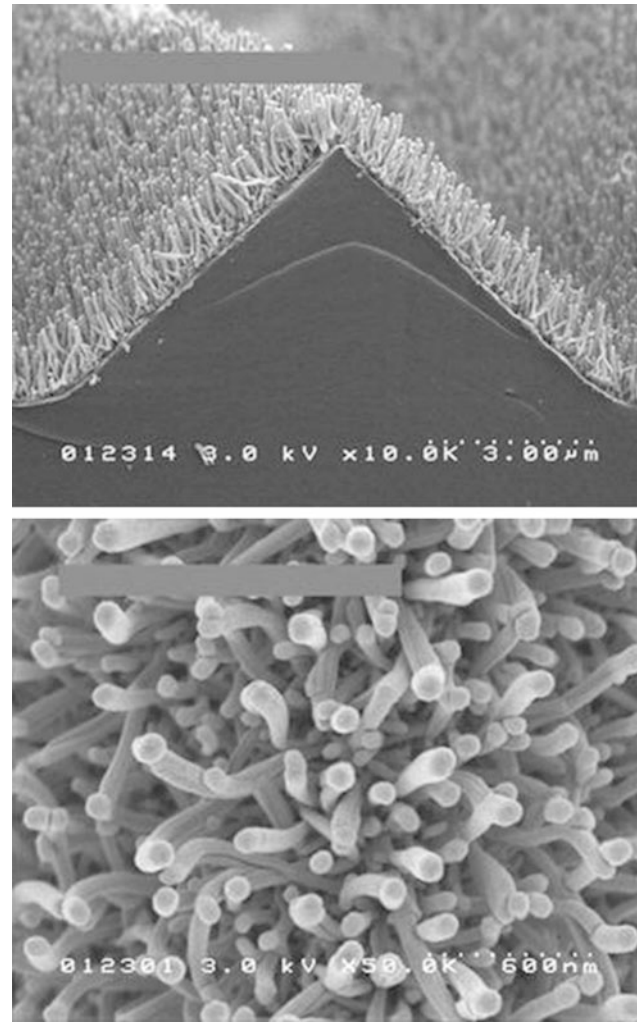

PEM Fuel Cells and Platinum-Based Electrocatalysts, Fig. 10 Scanning electron micrographs of typical NSTF catalysts as fabricated on a microstructured catalyst transfer substrate, seen (*top*) in cross section with original magnification of ×10,000, and (*bottom*) in plain view with original magnification of ×50,000. The dotted scale bar is shown in each micrograph (Reproduced from [127] with permission)

temperature. The Pt-specific activity of the Pt/NSTF was found to be close to that of a Pt polycrystalline disk. A twofold gain of Pt specific activity was observed on Pt-Co-Mn/NSTF versus Pt/NSTF. In PEMFC measurements for the same loading of 0.2 mg Pt/cm^2, using GM recommended conditions for measuring specific and mass activity at 80 °C, saturated H_2/O_2 at 150 kPa_{abs}, at 900 mV, the NSTF Pt-Co-Mn catalyst-coated membrane (CCM) generated specific activities of 2.93 mA/cm^{2}Pt, and mass activities of 0.18 A/mg^1 Pt. The specific activity is <12 times higher, and mass activity is about two times higher than those of TKK 47 wt% Pt/C.

To investigate the NSTF electrode stability under high voltage cycling, Debe et al. [129] tested a series of NSTF Pt and NSTF Pt-ternary catalysts along with Pt/C (Ketjen Black) and Pt/C (graphitic) types by scanning at 20 mV/s, between 0.6 and 1.2 V under saturated H_2/N_2 at 80 °C. The MEA's contained the same 3 M-ionomer PEM having a 1000 equivalent weight (EW), and the same 3 M-coated GDL. The NSTF electrodes had loadings of 0.1 mg/cm^2, while the carbon- and graphitic-carbon-supported catalysts had loadings of 0.4 mg/cm^2. Fig. 11 compares the normalized surface area as a function of the number of CV cycles for all the samples. It is interesting to note that for the NSTF samples the Pt and ternary catalysts behave similarly and lose approximately 30% of the surface area out to 14,000 cycles. The Pt/C and Pt/graphitic carbon, on the other hand, lose substantially more surface area in significantly fewer cycles. The superior ability of the NSTF catalyst to withstand thousands of fast voltage scans over the potential range most critical for Pt dissolution and Pt agglomeration demonstrated a significant differentiating feature over carbon-supported catalysts [129].

Recently, Chen et al. [130] developed supportless Pt nanotubes (PtNTs) and Pt-alloy nanotubes (e.g., Pt-Pd alloy nanotubes (PtPdNTs)) as cathode catalysts for PEMFCs. PtNTs were synthesized by a galvanic replacement of silver nanowires (AgNWs) by following a similar method developed by Xia and coworkers [131, 132]. The AgNWs were synthesized using a polyol method [133] and were subsequently heated at reflux temperature with $Pt(CH_3COO)_2$ in an aqueous solution. For the preparation of PtPdNTs, mixed aqueous $Pt(CH_3COO)_2$ and $Pd(NO_3)_2$ solutions were used. The diameter (Fig. 12a, b) and length of AgNWs are about 40 nm and 10 μm, respectively. After Pt replacement, the diameter, wall thickness (Fig. 12c, d), and length of the PtNTs are about 40 nm, 6 nm, and 10 μm, respectively.

Chen et al. [130] tested the durability of these materials by cycling the electrode between 0 and

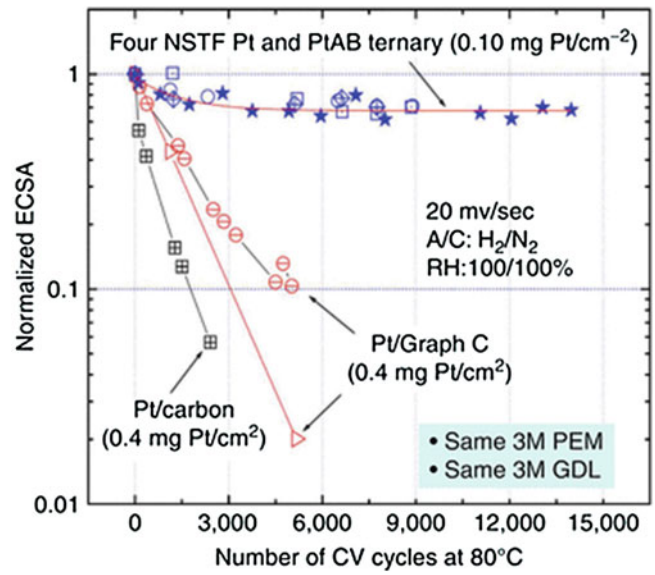

PEM Fuel Cells and Platinum-Based Electrocatalysts, Fig. 11 Normalized surface area versus number of CV cycles from 0.6 to 1.2 V for four NSTF catalyst samples and three Pt/carbon catalysts at 80°C. All MEAs used the same 3 M ionomer PEM and GDL (gas diffusion layer) (Reproduced from [129] with permission)

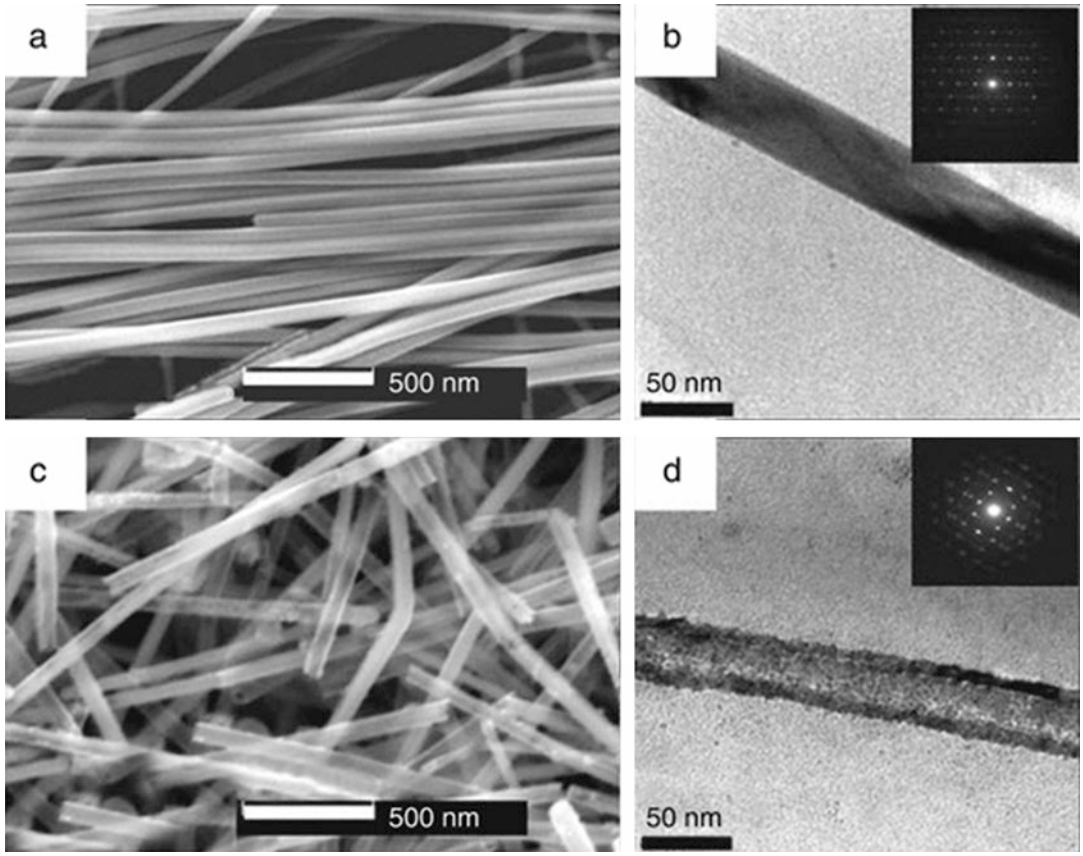

PEM Fuel Cells and Platinum-Based Electrocatalysts, Fig. 12 (**a**) SEM image of AgNWs. (**b**) TEM image and electron diffraction pattern (inset) of AgNWs. (**c**) SEM image of PtNTs. (**d**) TEM image and electron diffraction pattern (inset) of PtNTs (Reproduced from [130] with permission)

1.3 V versus RHE at a scan rate of 50 mV/s in argon-purged 0.5 M H_2SO_4 solution at 60 °C. As shown in Fig. 13a, the electrochemical surface area (ECSA) of the PtNTs decreased by about 20% after 1000 cycles, while the Pt-black and Pt/C catalysts lost about 51% and 90% of their platinum ECSA, respectively. Fig. 13b shows the comparison of typical ORR polarization curves of the respective catalysts obtained at room temperature in O_2-saturated 0.5 M H_2SO_4 using a rotating disk electrode (RDE) at 1600 rpm. At 0.85 V versus RHE, the mass activity of PtNTs was reported slightly higher than that of Pt/C, and 1.4 times higher than that of Pt-black catalysts. The specific activity of the PtNTs was 3.8 times and 1.8 times higher than those of Pt/C and Pt-black catalysts, respectively. For PtPdNTs, the mass activity was measured 1.4 times and 2.1 times higher than those of Pt/C and Pt-black catalysts, while the specific activity was 5.8 times and 2.7 times higher than those of Pt/C and Pt-black catalysts, respectively.

The examples given above illustrate that it is possible to achieve both activity and durability goals of Pt-based catalysts through special morphology and structural design of the catalyst and electrode. There are many other important advancements not discussed here on nanostructured Pt and Pt-alloy catalysts/electrodes showing improvements in activity and/or durability for ORR, such as single-crystal-Pt nanowires grown on continuous carbon-layer-coated Sn-fiber 3D electrodes [134], Pt-Pd bimetallic nanodendrites [135, 136], faceted Pt nanocrystals [137], nanoporous Pt alloy electrodes [138–140].

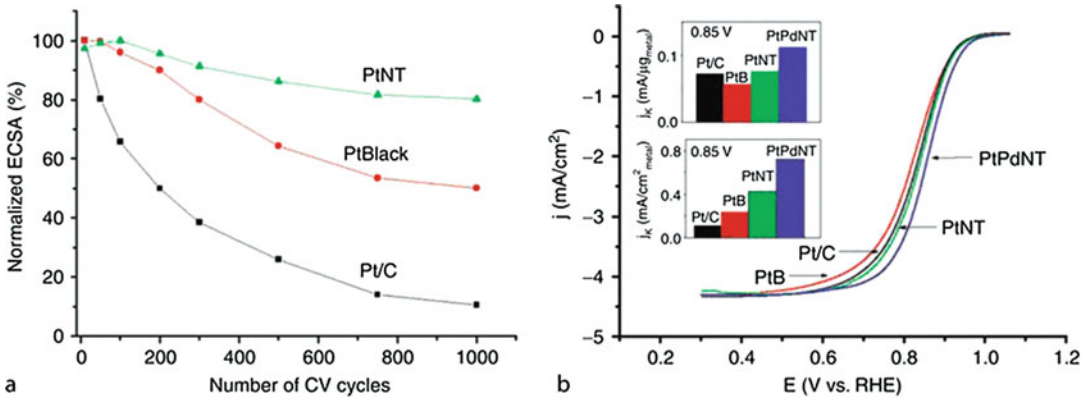

PEM Fuel Cells and Platinum-Based Electrocatalysts, Fig. 13 (**a**) Loss of electrochemical surface area (ECSA) of Pt/C (E-TEK), platinum-black (PtB; E-TEK), and PtNT catalysts with number of potential cycles in Ar-purged 0.5 M H_2SO_4 solution at 60°C (0-1.3 V versus RHE, sweep rate 50 mV/s). (**b**) ORR curves (shown as current-voltage relations) of Pt/C, platinum black (PtB), PtNTs, and PdPtNTs in O_2-saturated 0.5 M H_2SO_4 solution at room temperature (1,600 rpm, sweep rate 5 mV/s). Inset: Mass activity (*top*) and specific activity (*bottom*) for the four catalysts at 0.85 V (Reproduced from [130] with permission)

Facet- and Shape-Controlled Pt-Alloy Nanocrystal Electrocatalysts

Stamenkovic and coworkers [42] demonstrated in $HClO_4$ that on RDE $Pt_3Ni(111)$ single-crystal surfaces of <6 mm in diameter, the specific activity for ORR is about an order of magnitude higher than on the Pt(111) surface and is about 90 times higher than on Pt/C catalyst, while the other two low-index surfaces, [$Pt_3Ni(100)$ and $Pt_3Ni(110)$] are much less active than $Pt_3Ni(111)$. This result is very intriguing in that it suggests that if one can make Pt_3Ni nanocrystals with all exposed surfaces having {111} orientations, one can hope to gain an enhancement of specific activity by up to two orders of magnitude relative to state-of-the-art Pt/C catalysts. Recently, two interesting papers [141, 142] have shown progress on synthesizing such Pt alloy nanocrystals.

Wu et al. [141] recently reported an approach to the preparation of truncated-octahedral Pt_3Ni (*t,o*-Pt_3Ni) catalysts that have dominant exposure of {111} facets. The shape-defined Pt-Ni nanoparticles were made from platinum acetylacetonate [$Pt(acac)_2$] and nickel acetylacetonate [$Ni(acac)_2$] in diphenyl ether (DPE) using a mixture of borane-tert-butylamine complex (TBAB) and hexadecanediol as the reducing agents. Long-alkane-chain amines were used as the main capping agents, and adamantanecarboxylic acid (ACA) or adamantaneacetic acid (AAA) was used to affect the reaction kinetics. The population of truncated octahedral crystals could be adjusted by the types and amounts of the reducing agents and capping agents. Three sets of Pt_3Ni nanocrystals were generated with various truncated-octahedral crystal populations; see Fig. 14.

While Fig. 14a, b contain 30% and 10% of Pt_3Ni cubes (with the remaining particles being truncated-octahedrons), respectively, Fig. 14c contains only truncated-octahedrons. The particle size is on the order of 5 to 7 nm. Only two types of facets are exposed of all the nanocrystals, i.e., the {111} and {100}. The fractions of the {111} surface area over the total surface area could be calculated based on the geometries of the shapes and the population statistics. The ORR kinetics of the nanocrystals were studied on RDEs in O_2-saturated 0.1 M $HClO_4$, at room temperature, at 1600 rpm, with a potential scan rate of 10 mV/s. Fig. 15 shows comparison of polarization curves, cyclic-voltammetry curves, mass activities, and specific activities of the Pt3Ni nanocrystals to the standard TKK Pt/Vulcan carbon catalyst. As shown in Fig. 15d, almost-linear correlations were obtained for both mass activities and specific activities versus the fraction of the

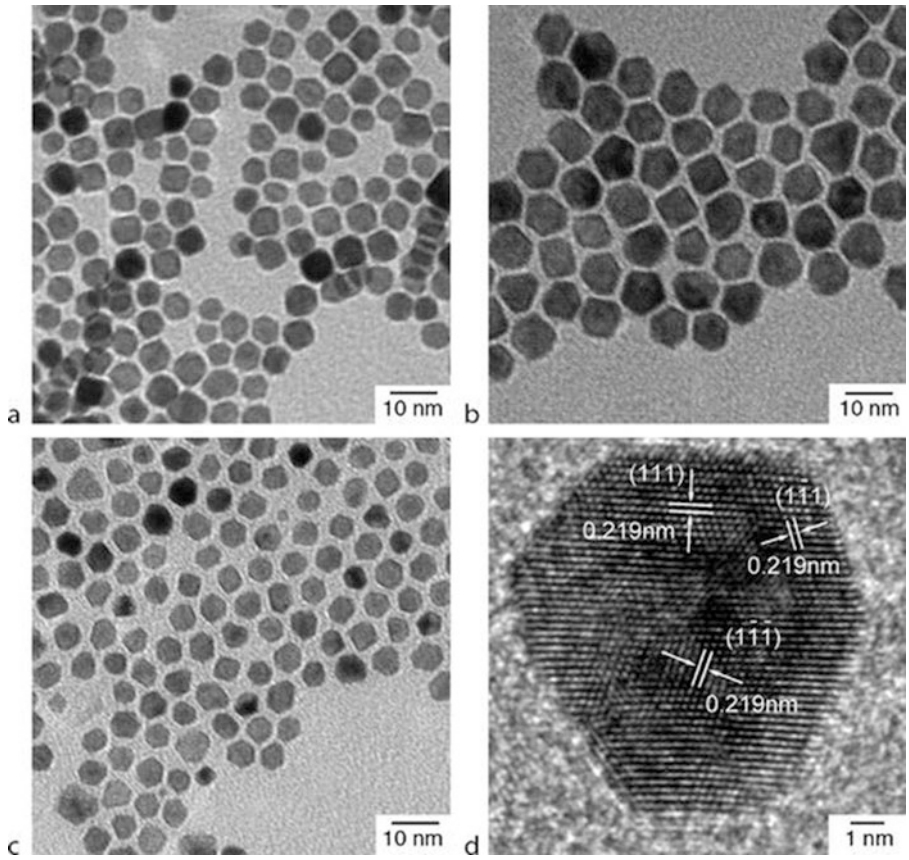

PEM Fuel Cells and Platinum-Based Electrocatalysts, Fig. 14 TEM images of Pt_3Ni nanocrystals with truncated octahedron population of (**a**) 70%, (**b**) 90%, (**c**) 100%, and (**d**) HR-TEM image of a truncated octahedron showing the (111) lattice (Reproduced from [141] with permission)

(111) surface area over the total surface area. A tabulated kinetic activity comparison is shown in Table 1. The mass activity and specific activity comparisons were made at 0.9 V versus RHE. Roughly 4× mass-activity and specific-activity enhancements were observed on the 100% truncated octahedral Pt_3Ni nanocrystals over the Pt/C catalyst. While the {111} facets of the nanocrystals showed much higher specific activity than the {100} facets, as indicated in Fig. 15d, in agreement with trend found on bulk Pt_3Ni single crystal disks, the absolute values of the specific activities of the nanocrystals are still far below those observed on bulk single-crystal surfaces [42].

Another interesting report is from Zhang et al. [142] on the synthesis and ORR activity of Pt_3Ni nano-octahedra and nanocubes, with the two shapes of nanocrystals having only {111} facets and {100} facets exposed, respectively. The monodispersed Pt_3Ni nano-octahedra and nanocubes were synthesized via a high-temperature organic solution chemistry approach, which involved using mixed oleylamine and oleic acid at elevated temperature as the reducing agent and capping agent, and tungsten hexacarbonyl $W(CO)_6$ as the shape controlling agent. Detailed procedures for synthesis of the nanocrystals can be found in Ref. [142]. Fig. 16 shows the SEM and TEM images of those shape and size controlled nano-octahedral (a-e) and nanocube (f-j) crystals. The chemical compositions of the crystals were analyzed by using combined ICP-MS and EDS techniques (from both TEM and SEM),

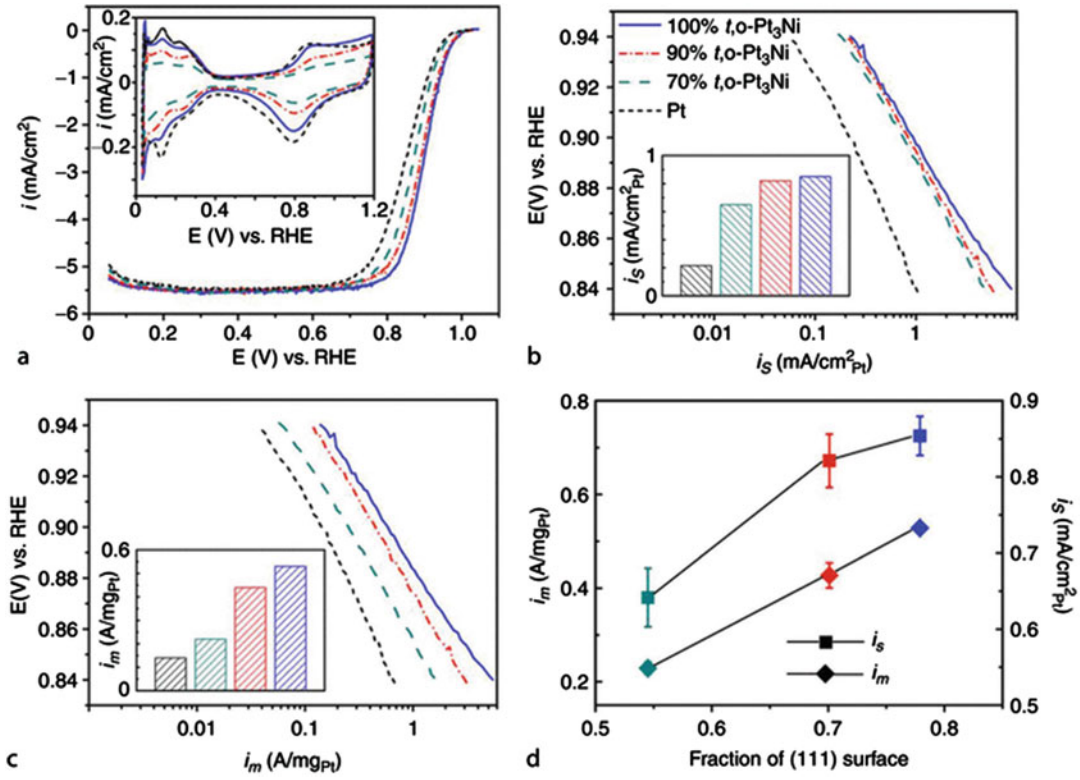

PEM Fuel Cells and Platinum-Based Electrocatalysts, Fig. 15 (**a**) Polarization curves and CV curves (*inset*), (**b**) area (mA/cm^{2}Pt), (**c**) mass (A/mg Pt) specific ORR activity for the *t,o*-Pt_3Ni and reference Pt catalysts; and (**d**) the correlations between specific activities and fractions of (111) surfaces of these Pt_3Ni catalysts. The ORR polarization curves were collected at 1,600 rpm (Reproduced from [141] with permission)

PEM Fuel Cells and Platinum-Based Electrocatalysts, Table 1 ECSA, mass- and area- specific ORR activities of Pt_3Ni and Pt/catalysts (at 0.9 V versus RHE) (Reproduced from [141] with permission)

Sample name	Pt loading [μg_{Pt}/cm$^2_{disk}$]	ECSA [m^2/g_{Pt}]	Mass activity [A/mg_{Pt}]	Specific activity [mA/cm$^2_{Pt}$]
100% *t,o*-Pt_3Ni	9.3	62.4	0.53	0.85
90% *t,o*-Pt_3Ni	9.3	53.7	0.44	0.82
70% *t,o*-Pt_3Ni	9.3	33.8	0.22	0.65
Pt/C (TKK)	11	65	0.14	0.215

and the results suggested that the average molar ratio of Pt over Ni was 3:1.

Zhang et al. [142] further investigated ORR activities of the shape controlled nanocrystals by using RDE measurements. The ORR measurements were conducted in an O_2-saturated 0.1 M $HClO_4$ solution at 295 K. A characteristic set of polarization curves at 900 rpm for the ORR on Pt3Ni nano-octahedra, Pt3Ni nanocubes, and Pt nanocubes are displayed in Fig. 17a. After mass transport correction using Koutecky-Levich equation, and normalizing by the Pt surface area and mass, the kinetic activities (specific activity and mass activity) at 0.9 V were plotted in Fig. 17b. The Pt-specific activity of Pt_3Ni nano-octahedra were determined to be 5.1 times of that of the

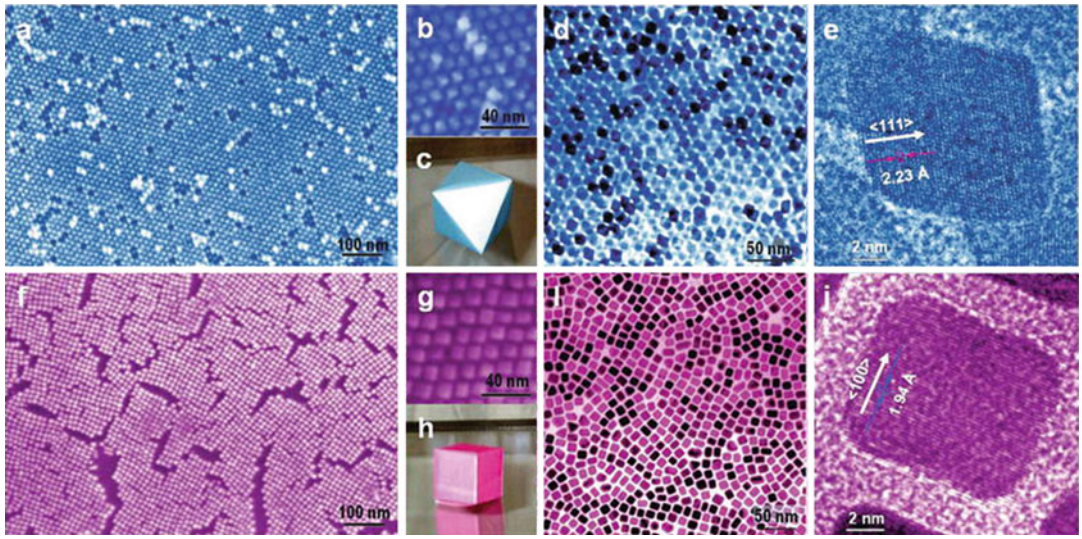

PEM Fuel Cells and Platinum-Based Electrocatalysts, Fig. 16 (**a**-**e**) Images for Pt_3Ni nano-octahedra. (**f**-**j**) Images for Pt_3Ni nanocubes. (**a**, **f**) Field-emission SEM images. (**b**, **g**) High-resolution SEM images. (**c**) 3D model of an octahedron. (**d**, **i**) TEM images. (**e**, **j**) High-resolution TEM images of single nanocrystals. (**h**) 3D model of a cube (Reproduced from [142] with permission)

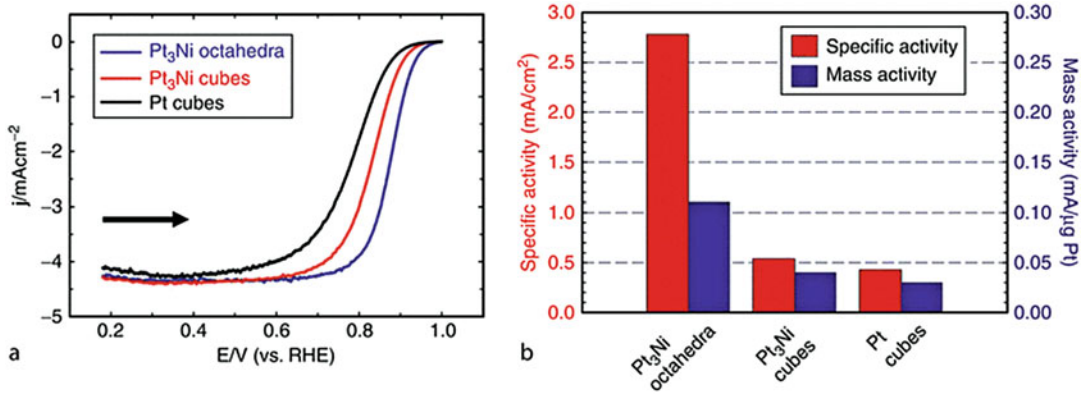

PEM Fuel Cells and Platinum-Based Electrocatalysts, Fig. 17 (**a**) Polarization curves for ORR on Pt_3Ni nano-octahedra, Pt_3Ni nanocubes, and Pt nanocubes supported on a rotating glassy carbon disk electrode in O_2-saturated 0.1 M $HClO_4$ solution at 295 K; with scan rate = 20 mV/s; rotation rate = 900 rpm. Catalyst loading in terms of Pt mass: Pt_3Ni octahedra, 3.0 μg; Pt_3Ni cube, 2.0 μg; Pt cube, 1.1 μg. Current density was normalized to the glassy carbon geometric surface area (0.196 cm^2). The arrow indicates the potential scan direction. (**b**) Comparison of the ORR activities on the three types of catalysts. Specific activity and mass activity were all measured at 0.9 V versus RHE at 295 K (Reproduced from [142] with permission)

Pt_3Ni nanocubes and <6.5 times that of the Pt nanocubes, while the Pt mass activity of the Pt_3Ni nano-octahedra was <2.8 times of that of Pt_3Ni nanocubes and <3.6 times of that of Pt nanocubes. The significant shape dependence of ORR activity agreed with the observation from the extended Pt_3Ni single crystal surfaces, although the absolute values of specific activities observed on Pt_3Ni nanocubes and nano-octahedra were about four- to sevenfold lower than those reported in Ref. [42], respectively. One apparent puzzle in these reported results is that the Pt surface area or ECSA of the nanocrystals derived from the specific activity and mass activity

(ECSA per unit mass of Pt = mass activity/specific activity) is 5–10 times lower than one would expect from the size of particles revealed by SEM and TEM images. The discrepancy may come from the low utilization of the surface area because of impurities or from overlap of the non-supported nanocrystals. Another set of data for the high surface carbon supported those nanocrystals was reported in the online supporting information of the paper, and this showed a better agreement between measured ECSA and diameter to TEM, suggesting that particle aggregation caused the low area observed for the unsupported catalysts.

In summary, the size- and shape-controlled synthesis of nanocrystal Pt-based electrocatalysts has shown a promising path to high Pt-specific activity, although the absolute number of the activity is still not comparable to that observed on extended Pt alloy single-crystal surface, probably due to the size effect, residual impurities and defects in the nanocrystal surface, and incomplete formation of smooth, segregated Pt layers on the facet surfaces. The Pt mass activity achieved for the best case is already about four times higher than state-of-the-art Pt/C catalyst. If the core of the nanocrystals can be replaced with some corrosion-resistant material but keeping the surface of the Pt alloy shell still in {111} facets, one could expect a significant further reduction of the Pt loading required for the cathode catalyst. In addition, the size of the particles can be larger to gain the benefits of the particle size effect, as the Pt consumption is determined by the thickness of the shell. The durability of such nanocrystals could be expected to be high because of the lack of low-coordination atoms in their surfaces.

Future Directions

Low platinum loading, high activity, and more durable catalysts still remain as critical challenges for PEFCs for automotive applications. Further fundamental understanding of the correlations between activity, stability, and structural properties at the atomic level are most desired from both theoretical and experimental perspectives. Studies of the connections between the activities of controlled-facet-orientation nanoparticles and extended single-crystal surfaces would be helpful. Structure- and surface-controlled syntheses of catalysts (Pt monolayer catalysts, nanostructured catalysts and electrodes, size- and facet-controlled Pt alloy nanocrystals, combined with core-shell structure) should provide a practical viable path to achieving fuel cell catalyst loadings required for large-scale commercialization.

Bibliography

Primary Literature

1. Andujar JM, Segura F (2009) Fuel cells: history and updating. A walk along two centuries. Renew Sust Energ Rev 13(9):2309–2322
2. Grimes PG (2000) Historical pathways for fuel cells – the new electric century. IEEE Aerosp Electron Syst Mag 15(12):7–10
3. Appleby AJ (1990) From Sir William Grove to today: fuel cells and the future. J Power Sources 29(1–2):3–11
4. Perry ML, Fuller TF (2002) A historical perspective of fuel cell technology in the 20th century. J Electrochem Soc 149(7):S59–S67
5. Thomas CE (2009) Fuel cell and battery electric vehicles compared. Int J Hydrog Energy 34(15):6005–6020
6. Gottesfeld S (2007) Fuel cell techno-personal milestones 1984–2006. J Power Sources 171(1):37–45
7. Mathias MF, Makharia R, Gasteiger HA, Conley JJ, Fuller TJ, Gittleman CJ, Kocha SS, Miller DP, Mittelsteadt CK, Xie T, Yan SG, Yu PT (2005) Two fuel cell cars in every garage? Electrochem Soc Interface 14(3):24–35
8. Raistrick ID (1986) In: Zee JWV, White RE, Kinoshita K, Burney HS (eds) Diaphragms, separators, and ion-exchange membranes, the electrochemical society proceedings series. The Electrochemical Society, Pennington, p 172
9. Wilson MS, Gottesfeld S (1992) Thin-film catalyst layers for polymer electrolyte fuel cell electrodes. J Appl Electrochem 22(1):1–7
10. Wilson MS, Gottesfeld S (1992) High performance catalyzed membranes of ultra-low Pt loadings for polymer electrolyte fuel cells. J Electrochem Soc 139(2):L28–L30
11. Wilson MS, Valerio JA, Gottesfeld S (1995) Low platinum loading electrodes for polymer electrolyte fuel-cells fabricated using thermoplastic ionomers. Electrochim Acta 40(3):355–363
12. Conway BE, Tilak BV (2002) Interfacial processes involving electrocatalytic evolution and oxidation of H-2, and the role of chemisorbed H. Electrochim Acta 47(22–23):3571–3594
13. Gasteiger HA, Markovic NM, Ross PN (1995) H_2 and CO electrooxidation on well-characterized Pt, Ru, and

Pt-Ru.2. rotating disk electrode studies of CO/H_2 mixtures at 62-degrees C. J Phys Chem 99(45): 16757–16767
14. Mukerjee S, McBreen J (1996) Hydrogen electrocatalysis by carbon supported Pt and Pt alloys – an in situ x-ray absorption study. J Electrochem Soc 143(7):2285–2294
15. Neyerlin KC, WB G, Jorne J, Gasteiger HA (2007) Study of the exchange current density for the hydrogen oxidation and evolution reactions. J Electrochem Soc 154(7):B631–B635
16. Tarasevich MR, Sadkowski A, Yeager E (1983) Oxygen electrochemistry. In: Conway BE, Bockris JO, Yeager E, Khan SUM, White RE (eds) Comprehensive treatise in electrochemistry. Plenum Press, New York, p 301
17. Adzic RR (1998) Recent advances in the kinetics of oxygen reduction. In: Lipkowski J, Ross PN (eds) Electrocatalysis. Wiley-VCH, New York, pp 197–241
18. Kinoshita K (1992) Electrochemical oxygen technology. Wiley, New York
19. Markovic NM, Gasteiger HA, Ross PN (1995) Oxygen reduction on platinum low-index single-crystal surfaces in sulfuric-acid-solution – rotating ring-Pt(Hkl) disk studies. J Phys Chem 99(11):3411–3415
20. Gasteiger HA, Panels JE, Yan SG (2004) Dependence of PEM fuel cell performance on catalyst loading. J Power Sources 127(1–2):162–171
21. Gasteiger HA, Kocha SS, Sompalli B, Wagner FT (2005) Activity benchmarks and requirements for Pt, Pt-alloy, and non-Pt oxygen reduction catalysts for PEMFCs. Appl Catal B Environ 56(1–2):9–35
22. Damjanovic A, Brusic V (1967) Electrode kinetics of oxygen reduction on oxide-free platinum electrodes. Electrochim Acta 12(6):615–628
23. Wang JX, Markovic NM, Adzic RR (2004) Kinetic analysis of oxygen reduction on Pt(111) in acid solutions: intrinsic kinetic parameters and anion adsorption effects. J Phys Chem B 108(13):4127–4133
24. Markovic NM, Gasteiger HA, Grgur BN, Ross PN (1999) Oxygen reduction reaction on Pt(111): effects of bromide. J Electroanal Chem 467(1):157–163
25. Adzic RR (1992) Surface morphology effects in oxygen electrochemistry. In: Scherson D, Tryk D, Xing X (eds) Proceedings of the workshop on structural effects in electrocatalysis and oxygen electrochemistry. The Electrochemical Society, Pennington, p 419
26. Uribe FA, Wilson MS, Springer TE, Gottesfeld S (1992) Oxygen reduction (ORR) at the Pt/recast ionomer interface and some general comments on the ORR at Pt/aqueous electrolyte interfaces. In: Scherson DD, Tryk D, Xing X (eds) Proceedings of the workshop on structural effects in electrocatalysis and oxygen electrochemistry. The Electrochemical Society, Pennington, p 494
27. Norskov JK, Rossmeisl J, Logadottir A, Lindqvist L, Kitchin JR, Bligaard T, Jonsson H (2004) Origin of the overpotential for oxygen reduction at a fuel-cell cathode. J Phys Chem B 108(46):17886–17892
28. Wang JX, Zhang JL, Adzic RR (2007) Double-trap kinetic equation for the oxygen reduction reaction on Pt(111) in acidic media. J Phys Chem A 111(49): 12702–12710
29. Wang JX, Uribe FA, Springer TE, Zhang JL, Adzic RR (2008) Intrinsic kinetic equation for oxygen reduction reaction in acidic media: the double Tafel slope and fuel cell applications. Faraday Discuss 140:347–362
30. Neyerlin KC, WB G, Jorne J, Gasteiger HA (2006) Determination of catalyst unique parameters for the oxygen reduction reaction in a PEMFC. J Electrochem Soc 153(10):A1955–A1963
31. Neyerlin KC, Gu W, Jorne J, Clark A, Gasteiger HA (2007) Cathode catalyst utilization for the ORR in a PEMFC – analytical model and experimental validation. J Electrochem Soc 154(2):B279–B287
32. Neyerlin KC, Gasteiger HA, Mittelsteadt CK, Jorne J, WB G (2005) Effect of relative humidity on oxygen reduction kinetics in a PEMFC. J Electrochem Soc 152(6):A1073–A1080
33. Blurton KF, Greenberg P, Oswin HG, Rutt DR (1972) The electrochemical activity of dispersed platinum. J Electrochem Soc 119(5):559–564
34. Peuckert M, Yoneda T, Betta RAD, Boudart M (1986) Oxygen reduction on small supported platinum particles. J Electrochem Soc 133(5):944–947
35. Kinoshita K (1990) Particle size effects for oxygen reduction on highly dispersed platinum in acid electrolytes. J Electrochem Soc 137(3):845–848
36. Ross PN (1986) Structure-property relations in noble metal electrocatalysis. In: The Gordon conference on chemistry at interfaces. Lawrence Berkeley Laboratory, Berkeley/Meriden, p LBL-21733
37. Ross PN (1980) Oxygen reduction on supported Pt alloys and intermetallic compounds in phosphoric acid. Final report prepared for the electric power research institute. Electric Power Research Institute, Palo Alto, September 1980
38. Sattler ML, Ross PN (1986) The surface structure of Pt crystallites supported on carbon black. Ultramicroscopy 20:21–28
39. Landsman DA, Luczak FJ (2003) Catalyst studies and coating technologies. In: Vielstich W, Gasteiger H, Lamm A (eds) Handbook of fuel cells. Wiley, Chichester, p 811
40. Thompsett D (2003) Pt alloys as oxygen reduction catalysts. In: Vielstich W, Gasteiger H, Lamm A (eds) Handbook of fuel cells – fundamentals, technology and applications. Wiley, Chichester, p 467
41. Markovic N, Gasteiger H, Ross PN (1997) Kinetics of oxygen reduction on Pt(hkl) electrodes: implications for the crystallite size effect with supported Pt electrocatalysts. J Electrochem Soc 144(5):1591–1597
42. Stamenkovic VR, Fowler B, Mun BS, Wang GF, Ross PN, Lucas CA, Markovic NM (2007) Improved oxygen reduction activity on Pt3Ni(111) via increased surface site availability. Science 315(5811):493–497
43. Hammer B, Norskov JK (2000) Theoretical surface science and catalysis – calculations and concepts. In:

Gates BC, Knozinger H (eds) Advances in catalysis, vol 45. Academic, San Diego, pp 71–129
44. Norskov JK, Bligaard T, Logadottir A, Bahn S, Hansen LB, Bollinger M, Bengaard H, Hammer B, Sljivancanin Z, Mavrikakis M, Xu Y, Dahl S, Jacobsen CJH (2002) Universality in heterogeneous catalysis. J Catal 209(2):275–278
45. Lopez N, Janssens TVW, Clausen BS, Xu Y, Mavrikakis M, Bligaard T, Norskov JK (2004) On the origin of the catalytic activity of gold nanoparticles for low-temperature CO oxidation. J Catal 223(1):232–235
46. Xu Y, Mavrikakis M (2003) Adsorption and dissociation of O2 on gold surfaces: effect of steps and strain. J Phys Chem B 107(35):9298–9307
47. Xu Y, Ruban AV, Mavrikakis M (2004) Adsorption and dissociation of O2 on Pt-Co and Pt-Fe alloys. J Am Chem Soc 126(14):4717–4725
48. Greeley J, Rossmeisl J, Hellman A, Norskov JK (2007) Theoretical trends in particle size effects for the oxygen reduction reaction. Z Phys Chemie-Int J Res Phys Chem Chem Phys 221(9–10):1209–1220
49. Mukerjee S, McBreen J (1998) Effect of particle size on the electrocatalysis by carbon-supported Pt electrocatalysts: an in situ XAS investigation. J Electroanal Chem 448(2):163–171
50. Yano H, Inukai J, Uchida H, Watanabe M, Babu PK, Kobayashi T, Chung JH, Oldfield E, Wieckowski A (2006) Particle-size effect of nanoscale platinum catalysts in oxygen reduction reaction: an electrochemical and Pt-195 EC-NMR study. Phys Chem Chem Phys 8(42):4932–4939
51. Gasteiger HA, Markovic NM (2009) Just a dream-or future reality? Science 324(5923):48–49
52. Mukerjee S, Srinivasan S, Soriaga MP, McBreen J (1995) Role of structural and electronic-properties of Pt and Pt alloys on electrocatalysis of oxygen reduction – an in-situ Xanes and Exafs investigation. J Electrochem Soc 142(5):1409–1422
53. Wakabayashi N, Takeichi M, Uchida H, Watanabe M (2005) Temperature dependence of oxygen reduction activity at Pt-Fe, Pt-Co, and Pt-Ni alloy electrodes. J Phys Chem B 109(12):5836–5841
54. Paulus UA, Wokaun A, Scherer GG, Schmidt TJ, Stamenkovic V, Markovic NM, Ross PN (2002) Oxygen reduction on high surface area Pt-based alloy catalysts in comparison to well defined smooth bulk alloy electrodes. Electrochim Acta 47(22–23):3787–3798
55. Glass JT, Cahen JGL, Stoner GE, Taylor EJ (1987) The effect of metallurgical variables on the electrocatalytic properties of PtCr alloys. J Electrochem Soc 134(1):58–65
56. Paffett MT, Daube KA, Gottesfeld S, Campbell CT (1987) Electrochemical and surface science investigations of PtCr alloy electrodes. J Electroanal Chem 220(2):269–285
57. Beard BC, Ross JPN (1990) The structure and activity of Pt-Co alloys as oxygen reduction electrocatalysts. J Electrochem Soc 137(11):3368–3374
58. Toda T, Igarashi H, Uchida H, Watanabe M (1999) Enhancement of the electroreduction of oxygen on Pt alloys with Fe, Ni, and Co. J Electrochem Soc 146(10):3750–3756
59. Koh S, Hahn N, CF Y, Strasser P (2008) Effects of composition and annealing conditions on catalytic activities of dealloyed Pt-Cu nanoparticle electrocatalysts for PEMFC. J Electrochem Soc 155(12): B1281–B1288
60. Schulenburg H, Muller E, Khelashvili G, Roser T, Bonnemann H, Wokaun A, Scherer GG (2009) Heat-treated $PtCo_3$ nanoparticles as oxygen reduction catalysts. J Phys Chem C 113(10):4069–4077
61. Jalan V, Taylor EJ (1983) Importance of interatomic spacing in catalytic reduction of oxygen in phosphoric acid. J Electrochem Soc 130(11):2299–2302
62. Jalan V, Taylor EJ (1984) Importance of interatomic spacing in the catalytic reduction of oxygen in phosphoric acid. In: McIntyre JDE, Weaver MJ, Yeager EB (eds) The electrochemical society softbound proceedings series. The Electrochemical Society, Pennington, p 546
63. Landsman DA, Luczak FJ (1982) Noble metal-chromium alloy catalysts and electrochemical cell. US Patent 4,316,944, United Technologies Corporation: US
64. Stamenkovic VR, Mun BS, Arenz M, Mayrhofer KJJ, Lucas CA, Wang GF, Ross PN, Markovic NM (2007) Trends in electrocatalysis on extended and nanoscale Pt-bimetallic alloy surfaces. Nat Mater 6(3):241–247
65. Toda T, Igarashi H, Watanabe M (1999) Enhancement of the electrocatalytic O2 reduction on Pt-Fe alloys. J Electroanal Chem 460(1–2):258–262
66. M-k M, Cho J, Cho K, Kim H (2000) Particle size and alloying effects of Pt-based alloy catalysts for fuel cell applications. Electrochim Acta 45(25–26):4211–4217
67. Koh S, Strasser P (2007) Electrocatalysis on bimetallic surfaces: modifying catalytic reactivity for oxygen reduction by voltammetric surface dealloying. J Am Chem Soc 129(42):12624
68. Gottesfeld S (1986) The ellipsometric characterization of Pt + Cr alloy surfaces in acid solutions. J Electroanal Chem 205(1–2):163–184
69. Paffett MT, Beery JG, Gottesfeld S (1988) Oxygen reduction at $Pt_{0.65}Cr_{0.35}$, $Pt_{0.2}Cr_{0.8}$ and roughened platinum. J Electrochem Soc 135(6):1431–1436
70. Mukerjee S, Srinivasan S (1993) Enhanced electrocatalysis of oxygen reduction on platinum alloys in proton exchange membrane fuel cells. J Electroanal Chem 357(1–2):201–224
71. Toda T, Igarashi H, Watanabe M (1998) Role of electronic property of Pt and Pt alloys on electrocatalytic reduction of oxygen. J Electrochem Soc 145(12):4185–4188
72. Mun BS, Watanabe M, Rossi M, Stamenkovic V, Markovic NM, Ross PN (2005) A study of electronic structures of Pt3M (M = Ti, V, Cr, Fe, Co, Ni) polycrystalline alloys with valence-band photoemission spectroscopy. J Chem Phys 123(20):204717

73. Greeley J, Stephens IEL, Bondarenko AS, Johansson TP, Hansen HA, Jaramillo TF, Rossmeisl J, Chorkendorff I, Norskov JK (2009) Alloys of platinum and early transition metals as oxygen reduction electrocatalysts. Nat Chem 1(7):552–556
74. Mukerjee S, Srinivasan S, Soriaga MP, McBreen J (1995) Effect of preparation conditions of Pt Alloys on their electronic, structural, and electrocatalytic activities for oxygen reduction-XRD, XAS, and electrochemical studies. J Phys Chem 99(13):4577–4589
75. Uribe FA, Zawodzinski TA (2002) A study of polymer electrolyte fuel cell performance at high voltages. Dependence on cathode catalyst layer composition and on voltage conditioning. Electrochim Acta 47(22–23):3799–3806
76. Stamenkovic V, Schmidt TJ, Ross PN, Markovic NM (2002) Surface composition effects in electrocatalysis: kinetics of oxygen reduction on well-defined Pt3Ni and Pt3Co alloy surfaces. J Phys Chem B 106(46): 11970–11979
77. Murthi VS, Urian RC, Mukerjee S (2004) Oxygen reduction kinetics in low and medium temperature acid environment: correlation of water activation and surface properties in supported Pt and Pt alloy electrocatalysts. J Phys Chem B 108(30):11011–11023
78. Teliska M, Murthi VS, Mukerjee S, Ramaker DE (2005) Correlation of water activation, surface properties, and oxygen reduction reactivity of supported Pt-M/C bimetallic electrocatalysts using XAS. J Electrochem Soc 152(11):A2159–A2169
79. Lima FHB, Ticianelli EA (2004) Oxygen electrocatalysis on ultra-thin porous coating rotating ring/disk platinum and platinum-cobalt electrodes in alkaline media. Electrochim Acta 49(24):4091–4099
80. Lima FHB, Giz MJ, Ticianelli EA (2005) Electrochemical performance of dispersed Pt-M (M = V, Cr and Co) nanoparticles for the oxygen reduction electrocatalysis. J Braz Chem Soc 16(3 A):328–336
81. Lima FHB, Salgado JRC, Gonzalez ER, Ticianelli EA (2007) Electrocatalytic properties of PtCoC and PtNiC alloys for the oxygen reduction reaction in alkaline solution. J Electrochem So 154(4):A369–A375
82. Creemers C, Deurinck P (1997) Platinum segregation to the (111) surface of ordered $Pt_{80}Fe_{20}$: LEIS results and model simulations. Surf Interface Anal 25(3): 177–189
83. Gauthier Y, Joly Y, Baudoing R, Rundgren J (1985) Surface-sandwich segregation on nondilute bimetallic alloys: Pt50Ni50 and Pt78Ni22 probed by low-energy electron diffraction. Phys Rev B 31(10):6216–6218
84. Gauthier Y, Baudoing-Savois R, Bugnard JM, Hebenstreit W, Schmid M, Varga P (2000) Segregation and chemical ordering in the surface layers of $Pt_{25}Co_{75}$(111): a LEED/STM study. Surf Sci 466(1–3):155–166
85. Gasteiger HA, Ross PN Jr, Cairns EJ (1993) LEIS and AES on sputtered and annealed polycrystalline Pt-Ru bulk alloys. Surf Sci 293(1–2):67–80
86. Ruban AV, Skriver HL, Norskov JK (1999) Surface segregation energies in transition-metal alloys. Phys Rev B 59(24):15990–16000
87. Ma Y, Balbuena PB (2008) Pt surface segregation in bimetallic Pt3M alloys: a density functional theory study. Surf Sci 602(1):107–113
88. Chen S, Ferreira PJ, Sheng WC, Yabuuchi N, Allard LF, Shao-Horn Y (2008) Enhanced activity for oxygen reduction reaction on "Pt3CO" nanoparticles: direct evidence of percolated and sandwich-segregation structures. J Am Chem Soc 130(42):13818–13819
89. Stamenkovic VR, Mun BS, Mayrhofer KJJ, Ross PN, Markovic NM (2006) Effect of surface composition on electronic structure, stability, and electrocatalytic properties of Pt-transition metal alloys: Pt-skin versus Pt-skeleton surfaces. J Am Chem Soc 128(27): 8813–8819
90. Chen S, Sheng WC, Yabuuchi N, Ferreira PJ, Allard LF, Shao-Horn Y (2009) Origin of oxygen reduction reaction activity on "Pt3Co" nanoparticles: atomically resolved chemical compositions and structures. J Phys Chem C 113(3):1109–1125
91. Koh S, Leisch J, Toney MF, Strasser P (2007) Structure-activity-stability relationships of Pt-Co alloy electrocatalysts in gas-diffusion electrode layers. J Phys Chem C 111(9):3744–3752
92. Mani P, Srivastava R, Strasser P (2008) Dealloyed Pt-Cu core-shell nanoparticle electrocatalysts for use in PEM fuel cell cathodes. J Phys Chem C 112(7): 2770–2778
93. Srivastava R, Mani P, Hahn N, Strasser P (2007) Efficient oxygen reduction fuel cell electrocatalysis on voltammetrically dealloyed Pt-Cu-Co nanoparticles. Angew Chem Int Ed Engl 46(47):8988–8991
94. Neyerlin KC, Srivastava R, CF Y, Strasser P (2009) Electrochemical activity and stability of dealloyed Pt-Cu and Pt-Cu-Co electrocatalysts for the oxygen reduction reaction (ORR). J Power Sources 186(2): 261–267
95. Wang C, Van Der Vliet D, Chang KC, You H, Strmcnik D, Schlueter JA, Markovic NM, Stamenkovic VR (2009) Monodisperse Pt3Co nanoparticles as a catalyst for the oxygen reduction reaction: size-dependent activity. J Phys Chem C 113(45): 19365–19368
96. Watanabe M, Wakisaka M, Yano H, Uchida H (2008) Analyses of oxygen reduction reaction at Pt-based electrocatalysts. ECS Trans 16:199–206
97. Wakisaka M, Suzuki H, Mitsui S, Uchida H, Watanabe M (2008) Increased oxygen coverage at Pt-Fe alloy cathode for the enhanced oxygen reduction reaction studied by EC-XPS. J Phys Chem C 112(7): 2750–2755
98. Ferreira PJ, la OGJ, Shao-Horn Y, Morgan D, Makharia R, Kocha S, Gasteiger HA (2005) Instability of Pt/C electrocatalysts in proton exchange membrane fuel cells – a mechanistic investigation. J Electrochem Soc 152(11):A2256–A2271

99. Colon-Mercado HR, Popov BN (2006) Stability of platinum based alloy cathode catalysts in PEM fuel cells. J Power Sources 155(2):253–263
100. Morita T, Kojima K (2008) Development of fuel cell hybrid vehicle in Toyota. ECS Trans 16:185–198
101. Uchimura M, Sugawara S, Suzuki Y, Zhang J, Kocha SS (2008) Electrocatalyst durability under simulated automotive drive cycles. ECS Trans 16(2):225–234
102. Adzic RR, Zhang J, Sasaki K, Vukmirovic MB, Shao M, Wang JX, Nilekar AU, Mavrikakis M, Valerio JA, Uribe F (2007) Platinum monolayer fuel cell electrocatalysts. Top Catal 46(3–4):249–262
103. Brankovic SR, Wang JX, Adzic RR (2001) Pt submonolayers on Ru nanoparticles – a novel low Pt loading, high CO tolerance fuel cell electrocatalyst. Electrochem Solid State Lett 4(12):A217–A220
104. Sasaki K, Mo Y, Wang JX, Balasubramanian M, Uribe F, McBreen J, Adzic RR (2003) Pt submonolayers on metal nanoparticles – novel electrocatalysts for H2 oxidation and O2 reduction. Electrochim Acta 48(25–26):3841–3849
105. Wang JX, Brankovic SR, Zhu Y, Hanson JC, Adzic RR (2003) Kinetic characterization of PtRu fuel cell anode catalysts made by spontaneous Pt deposition on Ru nanoparticles. J Electrochem Soc 150(8):A1108–A1117
106. Brankovic SR, McBreen J, Adzic RR (2001) Spontaneous deposition of Pt on the Ru(0001) surface. J Electroanal Chem 503(1–2):99–104
107. Sasaki K, Wang JX, Balasubramanian M, McBreen J, Uribe F, Adzic RR (2004) Ultra-low platinum content fuel cell anode electrocatalyst with a long-term performance stability. Electrochim Acta 49(22–23):3873–3877
108. Kolb DM, Przasnyski M, Gerischer H (1974) Underpotential deposition of metals and work function differences. J Electroanal Chem 54(1):25–38
109. Herrero E, Buller LJ, Abruna HD (2001) Underpotential deposition at single crystal surfaces of Au, Pt, Ag and other materials. Chem Rev 101(7):1897–1930
110. Aramata A (1997) Underpotential deposition on single-crystal metals. In: Bockris JO, White RE, Conway BE (eds) Modern aspects of electrochemistry. Plenum, New York
111. Brankovic SR, Wang JX, Adzic RR (2001) Metal monolayer deposition by replacement of metal adlayers on electrode surfaces. Surf Sci 474(1–3): L173–L179
112. Zhang J, Mo Y, Vukmirovic MB, Klie R, Sasaki K, Adzic RR (2004) Platinum monolayer electrocatalysts for O2 reduction: Pt monolayer on Pd(111) and on carbon-supported Pd nanoparticles. J Phys Chem B 108(30):10955–10964
113. Zhang J, Vukmirovic MB, Sasaki K, Uribe F, Adzic RR (2005) Platinum monolayer electro catalysts for oxygen reduction: effect of substrates, and long-term stability. J Serb Chem Soc 70(3): 513–525
114. Zhang JL, Vukmirovic MB, Xu Y, Mavrikakis M, Adzic RR (2005) Controlling the catalytic activity of platinum-monolayer electrocatalysts for oxygen reduction with different substrates. Angew Chem Int Ed Engl 44(14):2132–2135
115. Zhang JL, Vukmirovic MB, Sasaki K, Nilekar AU, Mavrikakis M, Adzic RR (2005) Mixed-metal Pt monolayer electrocatalysts for enhanced oxygen reduction kinetics. J Am Chem Soc 127(36): 12480–12481
116. Zhou WP, Yang XF, Vukmirovic MB, Koel BE, Jiao J, Peng GW, Mavrikakis M, Adzic RR (2009) Improving electrocatalysts for O-2 reduction by fine-tuning the Pt-support interaction: Pt monolayer on the surfaces of a Pd3Fe(111) single-crystal alloy. J Am Chem Soc 131(35):12755–12762
117. Zhang J, Lima FHB, Shao MH, Sasaki K, Wang JX, Hanson J, Adzic RR (2005) Platinum monolayer on nonnoble metal-noble metal core-shell nanoparticle electrocatalysts for O2 reduction. J Phys Chem B 109(48):22701–22704
118. Zhang J, Sasaki K, Sutter E, Adzic RR (2007) Stabilization of platinum oxygen-reduction electrocatalysts using gold clusters. Science 315(5809): 220–222
119. Wang JX, Inada H, LJ W, Zhu YM, Choi YM, Liu P, Zhou WP, Adzic RR (2009) Oxygen reduction on well-defined core-shell nanocatalysts: particle size, facet, and pt shell thickness effects. J Am Chem Soc 131(47):17298–17302
120. Sasaki K, Wang JX, Naohara H, Marinkovic N, More K, Inada H, Adzic RR (2010) Recent advances in platinum monolayer electrocatalysts for oxygen reduction reaction: scale-up synthesis, structure and activity of Pt shells on Pd cores. Electrochim Acta 55(8):2645–2652
121. Shao-Horn Y, Sheng WC, Chen S, Ferreira PJ, Holby EF, Morgan D (2007) Instability of supported platinum nanoparticles in low-temperature fuel cells. Top Catal 46(3–4):285–305
122. PT Y, Gu W, Makharia R, Wagner FT, Gasteiger HA (2006) The impact of carbon stability on PEM fuel cell startup and shutdown voltage degradation. ECS Trans 3:797–809
123. Yu PT, Kocha S, Paine L, Gu W, Wagner FT (2004) The effects of air purge on the degradation of PEM fuel cells during startup and shutdown procedures. In: 2004 AIChE spring national meeting, conference proceedings, New Orleans, pp 521–527
124. Debe MK (2003) Novel catalyst, catalyst support and catalyst coated membrane methods. In: Vielstich W, Gasteiger HA, Lamm A (eds) Handbook of fuel cells – fundamentals technology and applications. Wiley, Chichester
125. Gancs L, Kobayashi T, Debe MK, Atanasoski R, Wieckowski A (2008) Crystallographic characteristics of nanostructured thin-film fuel cell electrocatalysts: a HRTEM study. Chem Mater 20(7): 2444–2454

126. Debe MK, Drube AR (1995) Structural characteristics of a uniquely nanostructured organic thin film. J Vac Sci Technol B Microelectron Nanometer Struct 13(3):1236–1241
127. Debe MK, Schmoeckel AK, Vernstrorn GD, Atanasoski R (2006) High voltage stability of nanostructured thin film catalysts for PEM fuel cells. J Power Sources 161(2):1002–1011
128. Bonakdarpour A, Stevens K, Vernstrom GD, Atanasoski R, Schmoeckel AK, Debe MK, Dahn JR (2007) Oxygen reduction activity of Pt and Pt-Mn-Co electrocatalysts sputtered on nano-structured thin film support. Electrochim Acta 53(2):688–694
129. Debe MK, Schmoeckel AK, Hendricks SM, Vernstrom GD, Haugen GM, Atanasoski RT (2005) Durability aspects of nanostructured thin film catalysts for PEM fuel cells. ECS Trans 1:51–66
130. Chen ZW, Waje M, Li WZ, Yan YS (2007) Supportless Pt and PtPd nanotubes as electrocatalysts for oxygen-reduction reactions. Angew Chem Int Edit Engl 46(22):4060–4063
131. Mayers B, Jiang X, Sunderland D, Cattle B, Xia Y (2003) Hollow nanostructures of platinum with controllable dimensions can be synthesized by templating against selenium nanowires and colloids. J Am Chem Soc 125(44):13364–13365
132. Sun Y, Tao Z, Chen J, Herricks T, Xia Y (2004) Ag nanowires coated with Ag/Pd alloy sheaths and their use as substrates for reversible absorption and desorption of hydrogen. J Am Chem Soc 126(19): 5940–5941
133. Sun Y, Yin Y, Mayers BT, Herricks T, Xia Y (2002) Uniform silver nanowires synthesis by reducing $AgNO_3$ with ethylene glycol in the presence of seeds and poly(vinyl pyrrolidone). Chem Mater 14(11):4736–4745
134. Sun SH, Zhang GX, Geng DS, Chen YG, Banis MN, Li RY, Cai M, Sun XL (2010) Direct growth of single-crystal Pt nanowires on Sn@CNT nanocable: 3D electrodes for highly active electrocatalysts. Chem Eur J 16(3):829–835
135. Peng ZM, Yang H (2009) Synthesis and oxygen reduction electrocatalytic property of Pt-on-Pd bimetallic heteronanostructures. J Am Chem Soc 131(22): 7542
136. Lim B, Jiang M, Camargo PHC, Cho EC, Tao J, Lu X, Zhu Y, Xia Y (2009) Pd-Pt bimetallic nanodendrites with high activity for oxygen reduction. Science 324(5932):1302–1305
137. Lim BW, XM L, Jiang MJ, Camargo PHC, Cho EC, Lee EP, Xia YN (2008) Facile synthesis of highly faceted multioctahedral Pt nanocrystals through controlled overgrowth. Nano Lett 8(11):4043–4047
138. Erlebacher J, Snyder J (2009) Dealloyed nanoporous metals for PEM fuel cell catalysis. ECS Trans 25:603–612
139. Zeis R, Mathur A, Fritz G, Lee J, Erlebacher J (2007) Platinum-plated nanoporous gold: an efficient, low Pt loading electrocatalyst for PEM fuel cells. J Power Sources 165(1):65–72
140. Erlebacher J (2009) Materials science of hydrogen/oxygen fuel cell catalysis. In: Ehrenreich H, Spaepen F (eds) Solid state physics – advances in research and applications. Academic, New York, pp 77–141
141. Wu J, Zhang J, Peng Z, Yang S, Wagner FT, Yang H (2010) Truncated octahedral Pt_3Ni oxygen reduction reaction electrocatalysts. J Am Chem Soc 132(14): 4984–4985
142. Zhang J, Yang H, Fang J, Zou S (2010) Synthesis and oxygen reduction activity of shape-controlled Pt3Ni nanopolyhedra. Nano Lett 10(2):638–644

Books and Reviews

Bard AJ, Faulkner LR (2001) Electrochemical methods, fundamentals and applications, 2nd edn. Wiley, New York

Lipkowski J, Ross P (eds) (1998) Electrocatalysis (frontiers in electrochemistry). Wiley-VCH, Danvers

Markovic NM, Ross PN Jr (2002) Surface science studies of model fuel cell electrocatalysts. Surf Sci Rep 45(4–6):117–229

Newman J, Thomas-Alyea KE (2004) Electrochemical system, 3rd edn. Wiley, Hoboken

Vielstich W, Gasteiger H, Lamm A (eds) (2003) Handbook of fuel cells: fundamentals, technology, applications. Wiley, Chichester

Vielstich W, Gasteiger H, Lamm A (eds) (2009) Handbook of fuel cells: advances in electrocatalysis, materials, diagnostics and durability, vol 5 and 6. Wiley, New York

Wieckowski A, Savinova ER, Vayenas CG (eds) (2003) Catalysis and electrocatalysis at nanoparticle surfaces, 1st edn. Boca Raton, CRC Press

Zhang J (ed) (2008) PEM fuel cell electrocatalysts and catalyst layers: fundamentals and applications, 1st edn. London, Springer